STUDIES ON PHOSPHATE AND SILANE COATINGS ON ALUMINUM ALLOY

by

JING FANG

B.Sc., Nanjing University, 1990

A THESIS SUBMITTED IN PARTIAL FULFILLMENT OF
THE REQUIREMENTS FOR THE DEGREE OF
MASTER OF SCIENCE

in

THE FACULTY OF GRADUATE STUDIES
Department of Chemistry

We accept this thesis as conforming
to the required standard

THE UNIVERSITY OF BRITISH COLUMBIA

April 1997

In presenting this thesis in partial fulfilment of the requirements for an advanced degree at the University of British Columbia, I agree that the Library shall make it freely available for reference and study. I further agree that permission for extensive copying of this thesis for scholarly purposes may be granted by the head of my department or by his or her representatives. It is understood that copying or publication of this thesis for financial gain shall not be allowed without my written permission.

Department of Chemistry

The University of British Columbia
Vancouver, Canada

Date May 14, 1997

DE-6 (2/88)

Abstract

The work in this thesis involves studies of two chromium-free corrosion protection coatings on 7075-T6 aluminum alloy. In Part I, emphasis was put on finding new coating recipes for forming an effective phosphate coating, while in Part II a search was made for evidence for direct Si-O-Al bonding at a particular organosilane/metal interface.

An initial review is made of the effects of changing parameters involved in forming a zinc phosphate coating layer by spraying. Various coatings were evaluated by X-ray photoelectron spectroscopy (XPS), scanning electron microscopy (SEM) and adhesion tests. The coating solution reported represents a modification of that previously used for coating the same system by the dipping method (J. Mat. Sci. **31** (1996) 565). For forming an adequate phosphate layer by spraying it was necessary to add the accelerators $KClO_3$ and $NaNO_2$, and to spray for 1 min. at 85°C (instead of 5 min. at 75°C for dipping). The polishing pre-treatment of the substrate also has a significant effect on the phosphate process: the coating formed on a surface polished by 1200 grit aluminum oxide sandpaper showed good adhesion to paint, whereas that polished with 1200 grit silicon carbide sandpaper, under otherwise identical conditions, failed to form an adhesive phosphate coating. In general, conditions for spraying are less easy to control than for dipping, but directions are indicated for obtaining promising coatings by the former approach.

The interface of γ-glycidoxypropyltrimethoxysilane (γ-GPS)/aluminum alloy was studied by the XPS bias potential technique and by secondary ion mass spectrometry (SIMS). Consistently with earlier work in this laboratory, a chemical shift was observed in narrow scan Al2p spectra from negatively biased samples, compared with those that were grounded (after correcting for the expected effect of the bias potential). The change in the electrical

properties of the aluminum oxide was previously hypothesized to indicate the presence of direct Si-O-Al interfacial bonding to the γ-GPS. In this thesis a further search was made to support this hypothesis by making static SIMS investigations of this interface. Samples which showed the bias potential effect also showed radicals at mass 71 in SIMS. Such species appear interpretable as $AlSiO^+$ and therefore are apparently indicative of direct Si-O-Al bonding at the interface.

Table of Contents

List of Tables

List of Figures

Acknowledgments

I would like to thank my supervisor, Professor K.A.R. Mitchell, for sponsoring this work and his advice and comments on this thesis. I am especially grateful to Dr. P.C. Wong for giving me a lot of helpful advice and guidance with XPS measurements. I would like to thank Dr. B.J. Flinn for much help with the SIMS investigation, and for teaching me about the computer programs for XPS and SIMS data processing, as well as trouble-shooting for all kinds of computer problems. I also thank Prof. M.Y. Zhou, Ms. Y.L. Leung, and Dr. J.F. Ying for sharing with me their knowledge and experience on the corrosion projects. I extend my gratitude to other members of the group: Ms. M. Kono, Dr. H. Wang, Mr. M. Saidy, Dr.W. Liu, Ms. D. Susac, Dr. Y.M. Wang, Dr. K.C. Wong and Ms. L. Shi. I also appreciate help from the Department of Physics for SEM measurements, and financial support for this program provided by the Department of National Defence.

Finally, I would like to thank my father, my brother and my husband, Yu-Luan Chen, for their endless love and continuous support throughout these years of my study. To them, I dedicated this thesis.

Chapter 1 Introduction

1.1 General

Ever since aluminum was first produced in 1855, the industry associated with aluminum and its alloys has seen an accelerating and notable expansion and development. Aluminum and its alloys are widely used for packaging, building, high strength materials for aircraft and automobiles, domestic and office applications, and a number of other industries [1]. These applications result from the distinctive features of this metal. Aluminum is one of the six most widely distributed metals on the surface of the earth. It is light (density 2.7 g/cm^3), it has a relatively high corrosion resistance, and it may achieve high mechanical strength by suitable alloying and heat treatments [2]. Still other valuable features are obtained by various treatments and finishings of aluminum and its alloys.

When a freshly formed surface of aluminum is exposed to the atmosphere, it is quickly covered with a thin oxide film. The excellent corrosion resistance of pure aluminum is largely due to this oxide film. However, this thin oxide film has only a limited thickness (e.g. about 2 to 3 nm at ambient temperature), and there is growing evidence that flaws pre-existing in the film can act as nucleation sites for film breakdown. The natural oxide film is not resistant to alkalis, and it may also be attacked by anions such as chlorides and sulfates. For aluminum alloys, the corrosion resistance shows a general decrease with increase in the alloying elements. Figure 1.1 shows the effect of corrosion on an aluminum alloy.

In order to improve the corrosion resistance and appearance of aluminum and its alloys, additional treatment processes are often needed. Such approaches include anodizing to thicken the oxide film, spraying another metal on the aluminum surface, or applying an

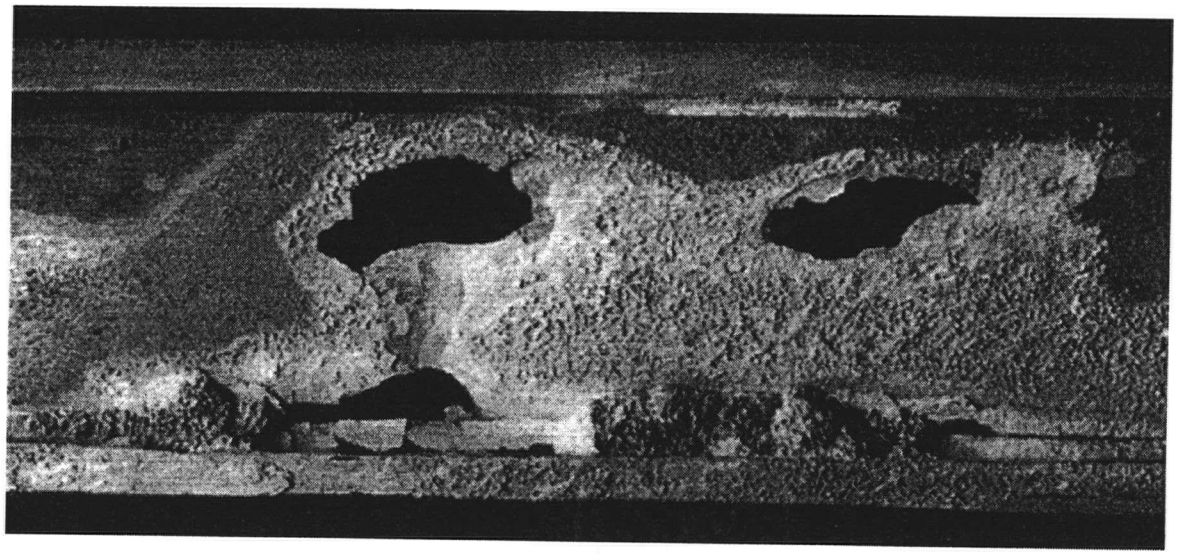

Figure 1.1 Corrosion on an Al 6063 alloy section [2]

organic coating [2]. Painting may be required for decorative, corrosion resistance, and other purposes but, since the naturally formed oxide film does not bond well directly to paints, primers are necessary. An effective primer adheres well to aluminum and its alloys, and permits good adhesion to the paint, so that it in effect serves to bond the paint to the metal surface. Chemical conversion coatings are often used as primers for aluminum. The term "chemical conversion coating" applies to the water insoluble inorganic coatings produced on metal surfaces by their external atomic layers reacting with the applied chemicals to give thin, tightly adherent films (often of a complex nature) which can provide an excellent and inexpensive paint base and an effective corrosion inhibiting layer [3].

Two types of chemical conversion coatings have been particularly important, namely those produced by chromating and by phosphating. The term "chromating" refers to the chemical or electrochemical treatments of metals and metallic coatings in solutions containing chromic acid, chromates or dichromates as the main constituents [4]. The conversion coatings produced on metal surfaces by such treatments are composed of Cr(III) and Cr(VI) compounds. Chromating provides a classic treatment for metals, and the first chromating process for aluminum was applied commercially in 1950 [5]. The high degree of anti-corrosion protection provided by the resulting coatings, and the simple method of processing have contributed to the widespread use of this process.

Although chromate coatings have excellent corrosion resistance and good adhesion for paints, the industrial usage of chromates is being increasingly restricted due to its toxicity, carcinogenic nature, and the resulting environmental impact. Phosphate coatings are suggested as a possible replacement [6]. Phosphate coatings have been widely applied to iron

and steel, and with some modification, it is believed that the phosphating process may also be useful for aluminum and its alloys.

1.2 Phosphating

The phosphating process gives a water insoluble phosphate coating on a metal surface by treating the metal with solutions containing phosphoric acid and heavy metal ions such as zinc, manganese, iron etc. Phosphate coatings can be applied on various metals such as iron, steel, zinc, aluminum, cadmium and manganese. Phosphating as we know it today is generally accepted as having originated from the work of Thomas W. Coslett in England, whose original patent, dated 1906 [7], covered the use of phosphoric acid to which iron filings were added. Today phosphate coatings are mainly used as a base for paint, and their commercial utilization is steadily increasing; for example a great part of the metal content in the world production of motorcars, bicycles, refrigerators, washing machines, office furniture, etc. is treated in this way [4].

A metal can form three types of phosphates, for example for Zn the specific formulas are:

$Zn(H_2PO_4)_2$	primary
$ZnHPO_4$	secondary
$Zn_3(PO_4)_2$	tertiary

Generally, the primary phosphates of heavy metals are soluble in water, the secondary phosphates are either insoluble or unstable and the tertiary phosphates are insoluble. The mechanism involved in the formation of phosphate coatings is quite complex, but all processes depend on the basic equilibria of the phosphoric acid:

$$H_3PO_4 = H^+ + H_2PO_4^- \quad (1.1)$$

$$H_2PO_4^- = H^+ + HPO_4^{2-} \quad (1.2)$$

$$HPO_4^{2-} = H^+ + PO_4^{3-} \quad (1.3)$$

The initiation of the coating formation process, for example on aluminum, involves phosphoric acid reacting with the metal substrate:

$$2Al + 6H^+ \rightarrow 2Al^{3+} + 3H_2\uparrow \quad (1.4)$$

The consumption of phosphoric acid in equation (1.4) lowers the acidity at the metal-solution interface, and shifts the equilibria positions in equations (1.1) to (1.3) to the right; consequently insoluble secondary and/or tertiary phosphate is deposited at the metal surfaces:

$$3Zn^{2+} + 2PO_4^{3-} \rightarrow Zn_3(PO_4)_2\downarrow \quad (1.5)$$

In principle, a phosphate solution can be applied for coating a metal surface either by dipping or by spraying. Commonly the dipping method is considered to provide more satisfactory phosphate coatings than the spraying method, and thus the former has gained more attention. However, the spraying method is more desirable for treating large pieces of metal (e.g. parts of a ship or aircraft) and it has its own advangages in some cases. For example, the study by Yonezaki et al [8] on the application of zinc phosphate solutions to electrogalvanised steel sheet suggested that the spraying method has the advantages of removing loosely adhered particles, and limiting the inclusion of bubbles on the metal surface during the phosphating process.

The chemical composition of phosphate coatings mainly consist of secondary and tertiary phosphates and metal oxides [9]. The coating, with thickness often in the range of 1 to 50 μm, can be either crystalline or amorphous, ideally with direct bonding to the metallic substrate [10]. In addition, the roughness and porosity of such coatings can provide an

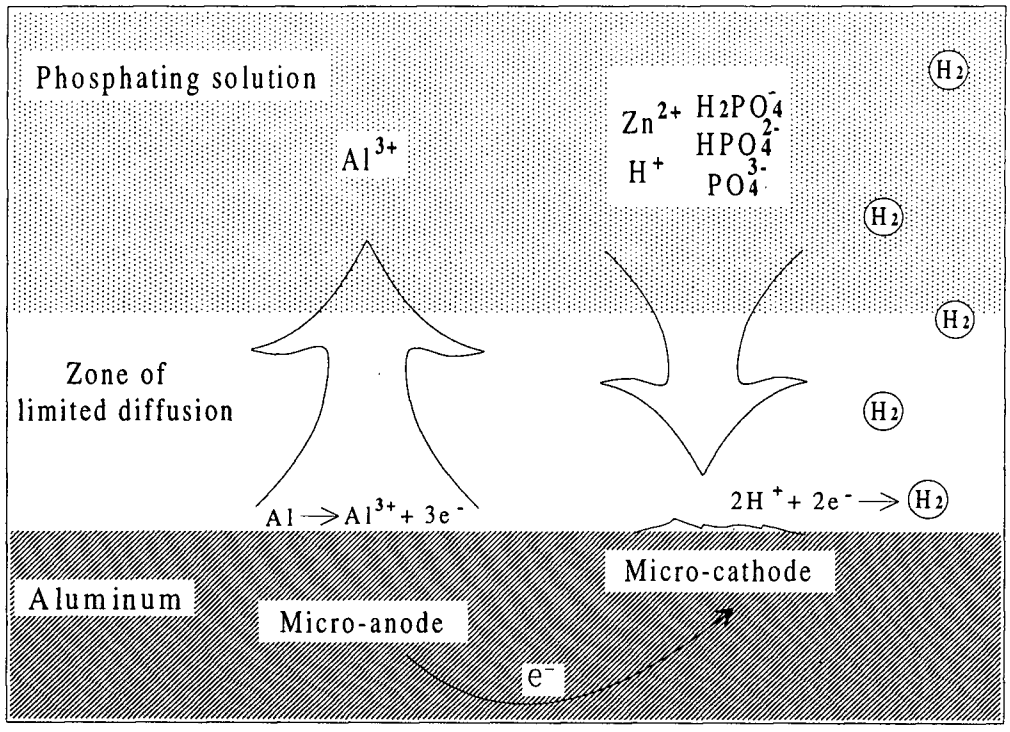

Figure 1.2 Schematic diagram of phosphating reaction for an aluminum sample. Phosphating is essentially an electrochemical phenomenon in which dissolution of metal occurs at the micro-anodes, and discharge of hydrogen followed by hydrolysis and precipitation of insoluble phosphates takes place at the micro-cathodes. (Modified after D.B. Freeman [15])

excellent basis for application of organic coatings, thereby improving the adhesion of these corrosion-protecting layers [11]. Finally, the phosphate coatings themselves can inhibit corrosion spread both from nearby corroded areas, and from areas where the organic coatings have been worn or damaged.

The composition and structure of phosphate coatings are influenced by a number of factors which may be summarized as follows:

1. Metal pre-treatment
2. Chemical composition of coating solution
3. Coating method (e.g. dipping or spraying) and working conditions (e.g. solution temperature and treatment time)

In order to produce a phosphate coating of good quality, the metal surface should be properly prepared before the phosphating treatment. The steps involved include removal of grease, an appropriate polishing, as well as a pre-treatment in an activating solution. Of considerable significance to the coating formation is the surface roughness of the metal, and the extent to which it has been mechanically worked. Generally very smooth metal surfaces give rise to coarser-grained and less regular phosphate coatings than those formed on roughened surfaces [1.2]. The finer coating structure on roughened surfaces, which is desirable, is normally formed due to the faster initial action by the free phosphoric acid, leading to a more rapid consumption of the acid at the solid-liquid interface. This in turn accelerates the nucleation process.

For the pre-treatment step, according to earlier research in this laboratory [13] and results from A.Turuno et al [14], activating surfaces of metals in solutions of titanium salts is effective for improving the quality of the phosphate coatings. It is believed that a membrane is formed by Ti-colloid pre-treatment. This activation leads to a reduction in the average

crystal grain size, and increases the coverage of the crystalline coating phase after the subsequent coating treatment. However, the details of how this membrane works still remain unclear.

Many efforts have been devoted to the development of appropriate coating solutions for phosphating on steel [15-18]. By contrast, much less research has been reported for aluminum and its alloys [19], and what is available is usually in the form of patents so that the detailed compositions and working conditions are not accessible. However, our laboratory has been investigating the chemistry of phosphate coating on aluminum alloy since 1991 and some useful results have been established. For example, the acidity of a phosphating solution plays a key role in the phosphating process. Free acid not only acts as a precursor in the coating formation, but also determines, to a large extent, the properties of the coating itself. Studies in our laboratory by W.F. Heung et al [20] and by J.F. Ying et al [21] have shown that the amounts of zinc and phosphorus in the resulted aluminum surface, as well as its corrosion resistance, are quite dependent on the acidity of the solution. The ZnO/H_3PO_4 ratio in the phosphating solution is an important factor which controls the amount of free acid as well as various kinds of phosphate ions, and consequently affects the resulted coating surfaces.

Working conditions such as bath temperature and treatment time also affect the resulting coatings. Studies by J.L. Fang et al [22] for dipping showed coatings formed at different bath temperatures and treatment times have different compositions and structures, and these parameters also affect the corrosion resistance.

Additionally, additives in the coating solution play an important role in the coating formation. For the phosphating of aluminum and its alloys, fluoride is commonly used in the coating solution [23-25]. Any free aluminum ions dissolved during the phosphating (see

equation (1.4)) will poison the zinc phosphate bath, but this can then be overcome by complexation:

$$Al^{3+} + 6F^{-} = (AlF_6)^{3-} \quad (1.6)$$

In practice, phosphating reactions tend to be slow owing to the evolution of hydrogen in the cathodic part of the reaction. In order to form phosphate coatings of good quality in reasonable times, accelerators are often used. The oxidizing accelerators are most important; they accelerate the coating formation reaction by reacting with hydrogen produced by equation (1.4) [26-28].

1.3 Characterization of phosphate coatings

Various instrumental techniques have been applied to study phosphate coatings and their properties [29]. X-ray diffraction (XRD) has been used to characterize the type and orientation of the major crystal phases present in phosphate coatings [30, 31]. This involves comparing diffraction patterns from coatings with those of reference crystals, but the approach has limited application to very fine-grained or amorphous coatings. For these measurements, coatings are stripped off the metal and the powders collected and studied. In consequence, the coatings are not measured in their original state, and it is hard to avoid damaging the metal-coating interface.

The nucleation and growth of phosphate crystals have been studied electrochemically by cathodic polarization [32, 33]. By measuring the current density during coating formation, the coverage of the coating can be inferred. However, this approach is indirect, and the interpretation of the results can be ambiguous.

Knowledge of chemical composition and chemical state of the elements in the phosphate coatings is particularly important for understanding their formation processes. More recently, X-ray photoelectron spectroscopy (XPS), a surface analytical technique, has emerged as a powerful aid in coating studies [34-37]. In essence, it involves the energy analysis of photoelectrons ejected from matter by incident X-rays. XPS has been applied to the investigation of surface properties of solid materials including catalysts, polymers and electronic materials [38]. XPS seems to be a very suitable technique for providing quantitative information on the chemical composition of phosphate coatings over its sampling depth (typically less than 100 Å). The interpretation of XPS spectra is relatively straightforward, and when combined with angle dependent measurements, it can also evaluate the distribution of elements with depth. Moreover, since XPS is a non-destructive method, the samples can be measured in their original states without being stripped off. This means that a sample can be measured non-destructively by XPS, and then probed further by a destructive method so as to obtain different types of information from the same sample.

The microtopography of a phosphated surface can be assessed by scanning electron microscopy (SEM), an important technique for surface imaging. Compared with an optical microscope, SEM images are produced by electrons reflected from the sample surface instead of light. The main advantages of SEM are provided by its spatial resolution (1-10 nm) and the large sampling depth (5-50 nm). This technique is useful for characterizing coating phases, grain morphology, grain size, grain distribution and uniformity of the coating [39-41].

Use of a combination of these surface analytical techniques should be particularly powerful in facilitating the study of interfacial coating reactions, and in assessing changes in morphological and chemical properties of the phosphate coatings for various pre-treatments,

coating solutions or substrates. The development of such knowledge should have great importance both theoretically and practically.

1.4 Aims of research

The motivation of the work originated from a contract with the Department of National Defence to help develop non-chromate coating processes for 7075-T6 aluminum alloy, a material used in airplane construction. Previous research in our group has been conducted on the phosphating of 7075-T6 aluminum alloy using the dipping method, and a satisfactory phosphating process has been developed [21]. However, sometimes for convenience and economy reasons, application of the coating by spraying would be advantageous (e.g. to repair part of an airplane without disassembly). The different application methods may result in coatings of very different crystal sizes, thicknesses or coverages, even with the same phosphating solution, therefore the coating process that works well with dipping may not produce good results for spraying. Accordingly there is a need to develop new coating processes for the spray coating of phosphate on to Al 7075-T6 alloy. For developing such a new process, factors such as chemical composition of the coating solution, working conditions and pre-treatment methods may all need to be re-considered. Phosphating reactions tend to be slowed by the generation of hydrogen gas as the metal is attacked by the phosphoric acid. This problem becomes more serious with spraying because the coatings need to form in a shorter period of time. In order to obtain phosphate coatings of good quality, accelerators, which were not used in our dipping process, need to be considered with spraying. And optimum working conditions also have to be determined. The investigation of such factors provides the first aim of the research reported in this thesis.

Once a sample has been phosphate coated by spraying, we need to evaluate the coatings obtained. This will involve characterization with regard to chemical composition and morphology by XPS and SEM. This defines the second aim of this work. The comparison of coatings formed at different conditions should help us understand more about the coating formation mechanism, and in turn that should guide the development of a suitable coating process by spraying.

The third aim of this research is to test the adhesive properties of the various coatings produced. Since a useful coating will be used as a primer for paint, its adhesion to paint is very important. Adhesion tests will be conducted for this purpose, and comparisons made between different coatings. This will help assess the effectiveness or otherwise for the different phosphating treatments.

Chapter 2 Characterization Techniques

2.1 X-ray photoelectron spectroscopy

2.1.1 Introduction

Analysis of a surface region for its chemical composition represents a particularly crucial characterization in surface science, and such information, along with geometrical structure, represents the most fundamental knowledge needed to understand the properties of a particular surface system. X-ray photoelectron spectroscopy (XPS) is one of the most widely used and powerful techniques for surface analysis [42]. XPS gives an elemental analysis (not H, He) for the top 20-100 Å of a solid surface, provided the material is vacuum stable. This technique can also provide chemical state information.

The XPS method has its origins in the discovery of photoemission by Hertz in 1887 [43] and its interpretation by Einstein in 1905 [44]. Initial development of this technique began with the early work of Robinson, Rawlinson and DeBroglie in the 1910s and 1920s [45]. The practical development of the technique was especially due to Siegbahn and co-workers in the early 1950s. They introduced a high resolution spectrometer for the detection of low-energy electrons produced by soft X-rays [46], and for this pioneering work in the area of photoelectron spectroscopy, Siegbahn shared the Nobel Prize in Physics in 1981 [47]. In 1972, Brundle and Roberts performed XPS studies on carefully prepared surfaces under ultrahigh vacuum conditions [48], and that work first established XPS as a surface analytical technique.

The basic XPS experiment is illustrated in Figure 2.1. A source of low-energy X-rays excites photoelectrons from a material, and the kinetic energies are measured with an energy analyzer. To a first approximation, the kinetic energy of a photoelectron is given by

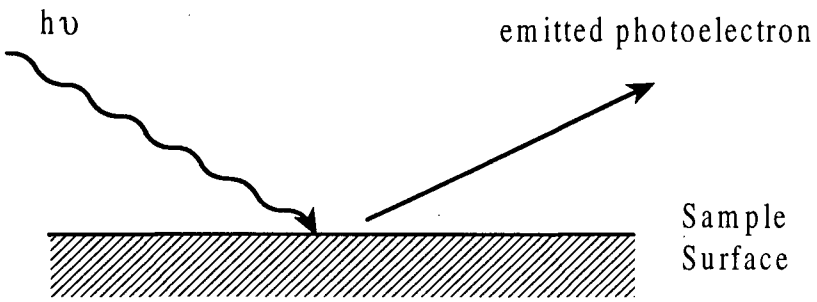

Figure 2.1 Schematic diagram showing the basic principle of the photoelectric effect

$$E_k = h\nu - E_b \quad (2.1)$$

where hν is the photon energy and E_b is the binding energy of the electron in the sample. Since different elements have different sets of electron binding energies, elemental identification is possible through measurement of the photoelectron kinetic energies. Figure 2.2 schematically shows the production of such a photoelectron, and additionally shows a de-excitation process associated with Auger emission. Again to a first approximation, the kinetic energy of the KL_1L_3 Auger electron is given by

$$E_{KL_1L_3} = E_k - E_{L_1} - E_{L_3} \quad (2.2)$$

where E_k, E_{L_1} and E_{L_3} are the binding energies of the levels involved.

Why is XPS a surface sensitive technique? To answer this question, consideration is needed for the inelastic mean free path (IMFP or λ) for an energetic electron inside a solid [49]. λ is defined as the average distance traveled by an electron in the material without energy loss, and it is a function of both the kinetic energy of the electron, and the material through which it is traveling. Figure 2.3 shows the general type of variation of λ with electron kinetic energy for many materials. Accordingly, for photoelectron kinetic energies in the range 100 to 1000 eV, values for λ of around 6 to 20 Å are common. The sampling depth of XPS is often indicated by 3λ, a distance from which 95% of an XPS signal is contributed. XPS is a surface sensitive technique therefore because of the high probability the photoelectrons have to experience inelastic scattering inside a solid.

Another view of inelastic scattering by electrons is indicated by Figure 2.4, which shows the number of scattered electrons, N(E), as a function of their exiting energy for an incident energy E_p. The peak of backscattered electrons (E = Ep) results from elastic

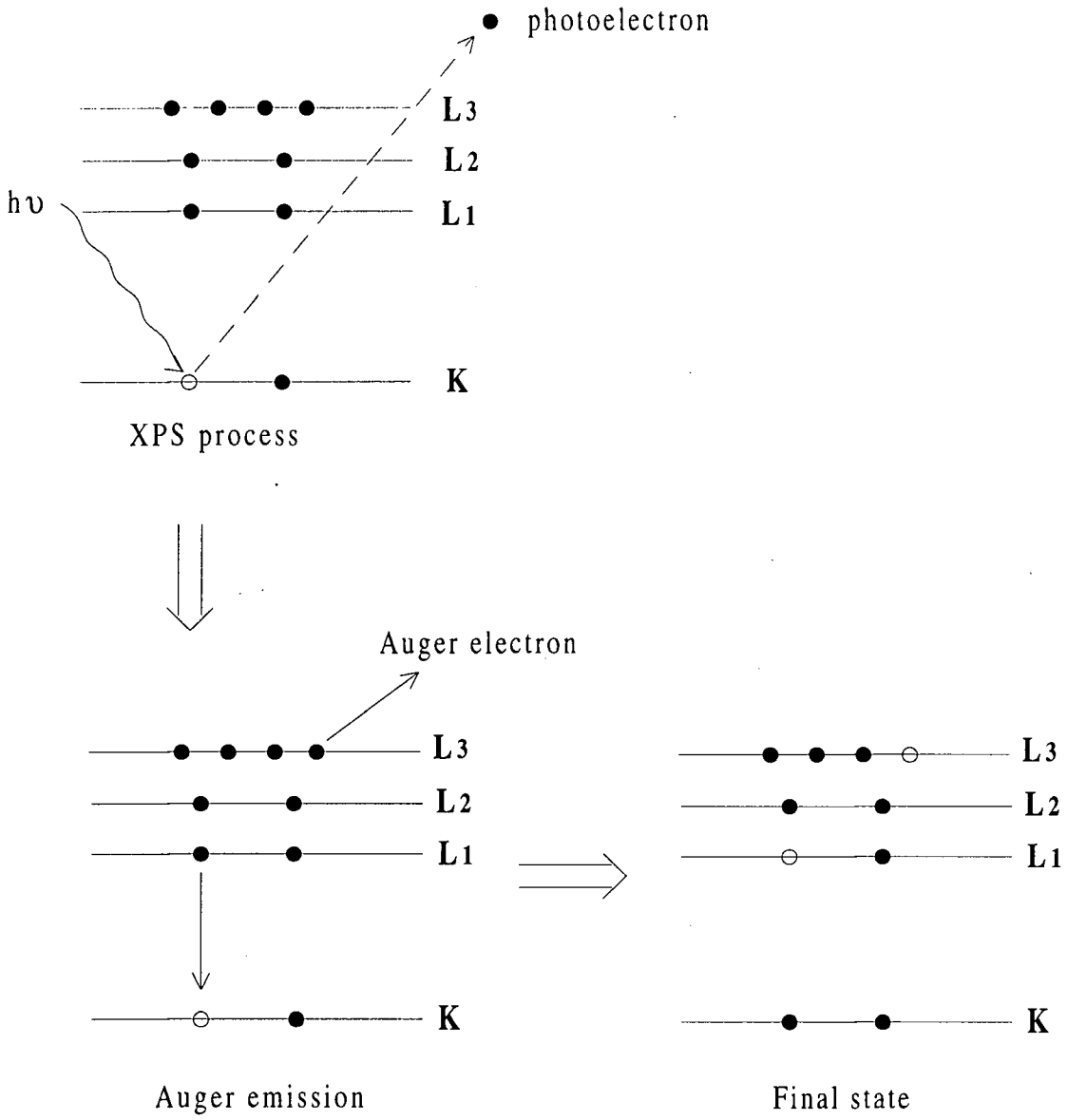

Figure 2.2 Schematic diagram for the XPS and Auger processes

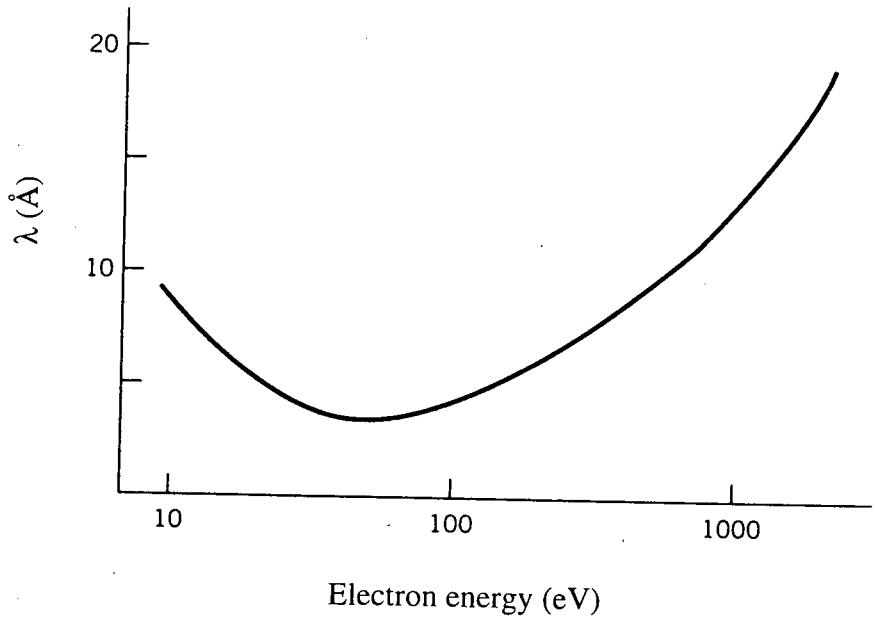

Figure 2.3 The IMFP as a function of the kinetic energy inside a solid [49].

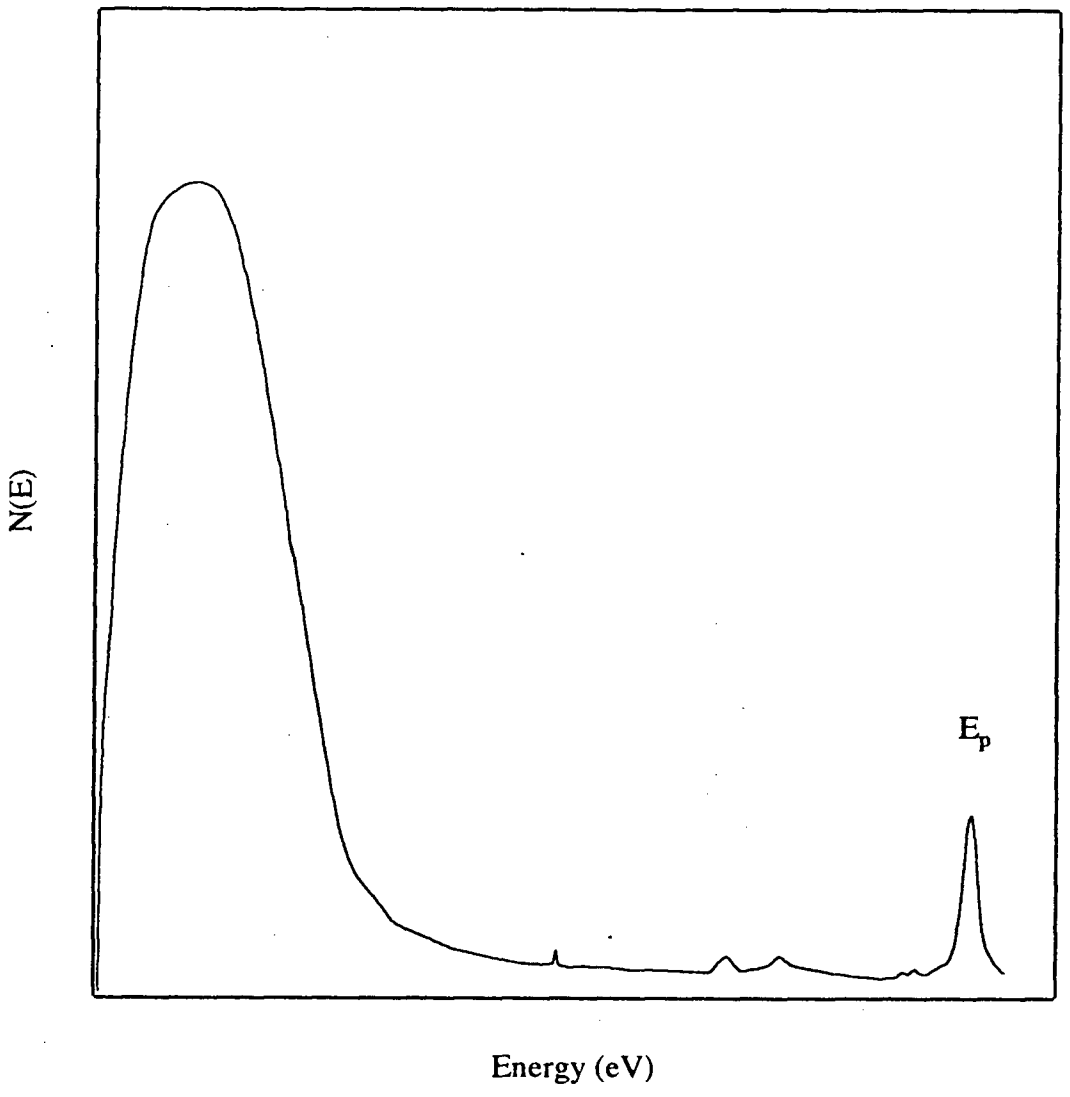

Figure 2.4 Schematic energy distribution N(E) of scattered electrons as a function of their exiting energy for primary energy E_p.

collisions while the large peak at low energies is due to secondary electrons created as a result of inelastic collisions between the incident electrons and electrons bound to the solid. For photoelectrons in XPS, probabilities for secondary emission are high, and such electrons contribute to the general background in a spectrum. However, in the scanning electron microscope (Section 2.3), it is the secondary electrons that are actively studied.

2.1.2 Instrumentation

XPS analyses reported in this thesis were made with a MAX200 facility (Leybold) which is shown in plan in Figure 2.5. The heart of this facility is the MAX200 spectrometer which comprises three main components, namely: (1) sample holders and manipulator, (2) X-ray source and (3) energy analyzer. All these components are held under ultra-high vacuum (UHV) (e.g. around 10^{-8} to 10^{-10} mbar). This is required to maintain a surface being studied in a constant state, but it is also needed to prevent unwanted collisions between the electrons to be analyzed and the ambient gas molecules, as well as for the reliable operation of some of the instrumentation (e.g. filaments, anodes, detector). The vacuum is achieved by an initial pumping to the 10^{-2} mbar range by rotary pumps, then turbomolecular pumps reduce the pressure down to around 10^{-8} mbar. The base pressure is achieved after "baking out" the whole UHV system at elevated temperature to desorb gas molecules from chamber walls and other surfaces. The pumping system for the MAX200 spectrometer is indicated schematically in Figure 2.6.

X-rays are generated by bombarding an anode material with electrons of sufficient energy. Choice of an anode material for XPS depends on three main considerations. The line width should not limit the energy resolution required, the X-ray intensity should be high, and

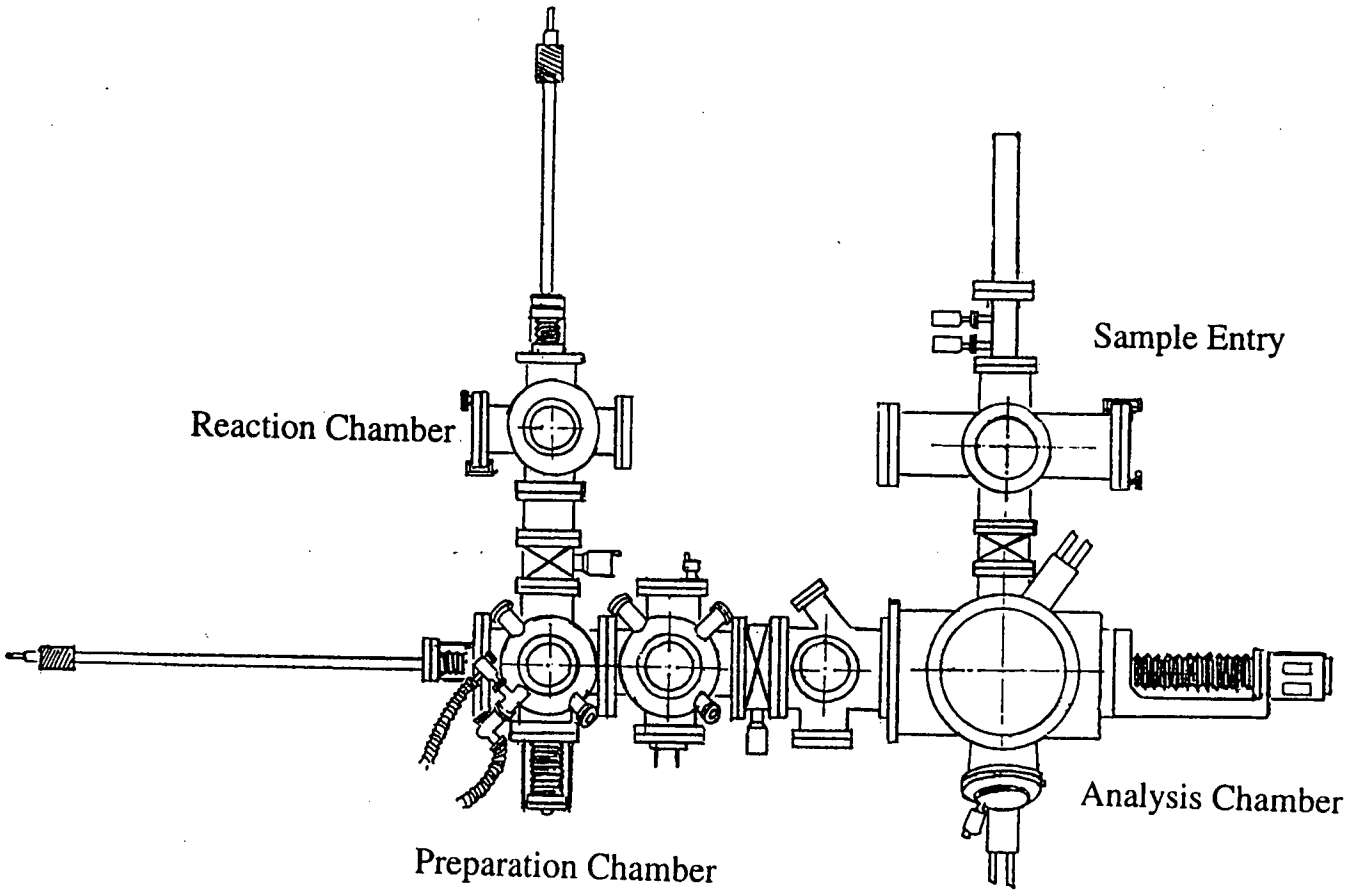

Figure 2.5 Top view of the MAX200 spectrometer.

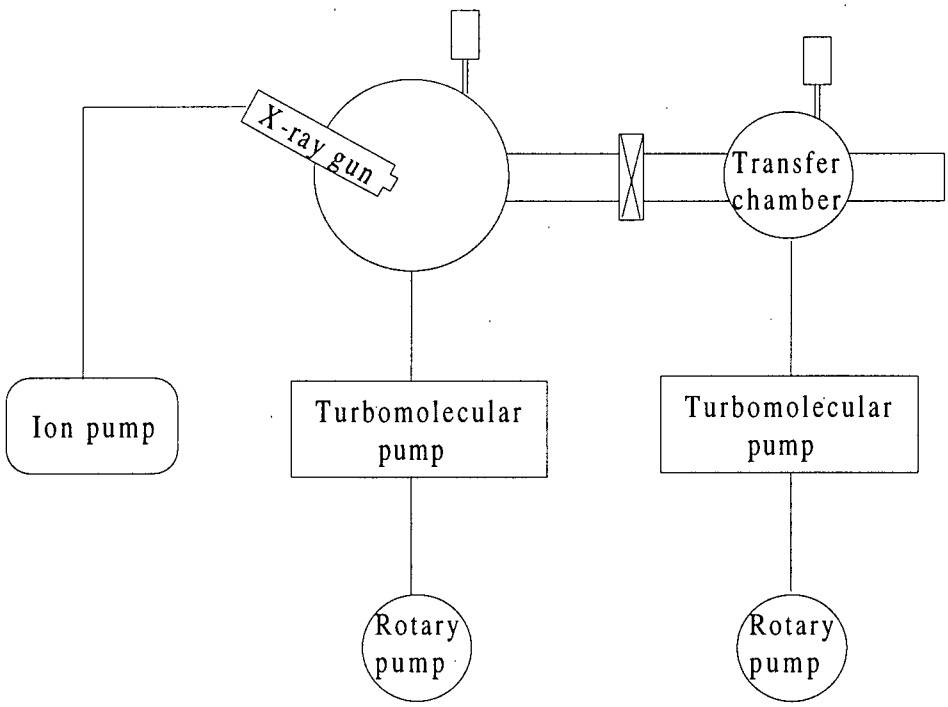

Figure2.6 Pumping system of MAX200 spectrometer

the energy should be sufficient that a reasonable range of photoelectron kinetic energies is available for analysis. The most commonly used X-ray sources are for the Kα lines of Mg and Al with energies of 1253.6 eV and 1486.6 eV respectively (these lines have respective widths of approximately 0.7 and 0.85 eV).

For XPS analysis in the MAX200, a set of samples are first mounted on holders, and up to seven of which can be locked on to a sample magazine in the sample entry chamber. The sample holders can then be transferred one at a time, under computer control, to the manipulator, which allows three linear and two rotational degrees of movement. These motions enable the sample to be appropriately positioned for the XPS analysis, including angle dependent measurement.

Energy analysis is done with an EA200 concentric hemispherical analyzer (CHA) (Figure 2.7). A retarding lens assembly, two concentric hemispheres and an electron detector make up the major components of the CHA. The retarding lens assembly is used to reduce the energy of the incoming electrons to the pass energy E_o, and the potential difference applied between the inner and outer hemispheres is such that only electrons with an energy close to E_o can pass through the analyzer and be detected at the position sensitive microchannel plate. The number of electrons within the energy band around E_o is then transferred to the computer, where the full signal intensity versus the retarding potential, and hence the kinetic energy of the incident electrons, is set up and stored [50].

The resolution of the energy analyzer varies with the chosen pass energy E_o. The smaller E_o, the better the energy resolution. However, the signal intensity drops off rapidly with decreasing pass energy. Therefore the pass energy should be chosen as a compromise between both resolution and intensity. The experimental resolution for a photoelectron

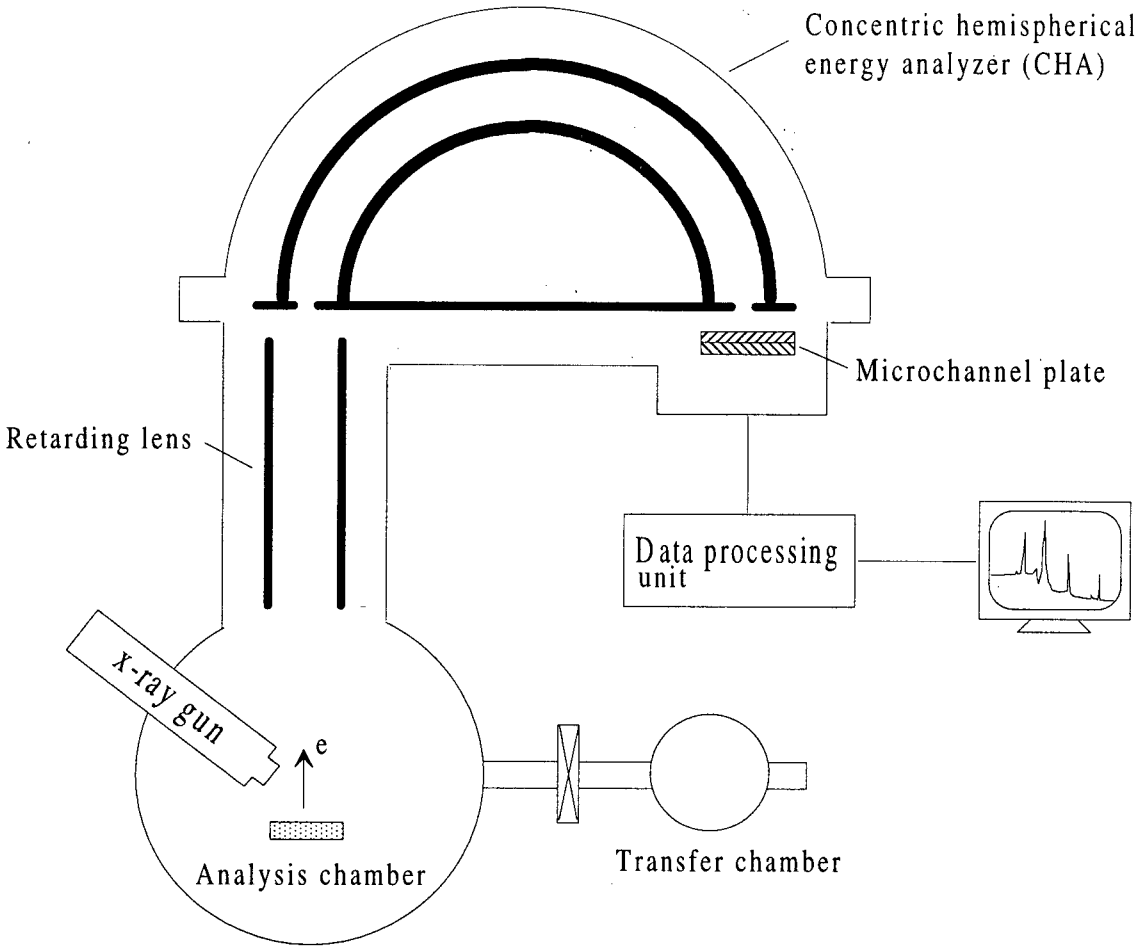

Figure 2.7 Schematic diagram showing the main components of the spectrometer.

peak, defined as the full width at half maximum (FWHM), is determined by three factors, namely the natural line of the X-ray source (ΔE_{source}), the resolution of energy analyzer ($\Delta E_{analyzer}$) and the inherent spectral width for the atomic level involved (ΔE_{line}). Assuming all contributions have a Gaussian shape, the observed width in a spectrum is given by:

$$FWHM_{total} = (\Delta E^2_{source} + \Delta E^2_{analyzer} + \Delta E^2_{line})^{1/2} \quad (2.3)$$

The kinetic energy of a photoelectron measured in the spectrometer (E_k') is referenced to the vacuum level of the spectrometer. In turn the binding energy E_b of the electron in the sample is referenced to the Fermi energy of the sample. For a conducting sample in electrical contact with the spectrometer (equal Fermi energies), Equation (2.1) needs modification to

$$E_k' = h\nu - E_b - W_{sp} \quad (2.4)$$

The spectrometer work function, W_{sp}, can be determined by calibration with standard samples; in general, it remains constant while the spectrometer is held under UHV. Equation (2.4) therefore enables photoelectron kinetic energies to be converted to binding energies. The spectra shown in this thesis have been calibrated against the $Au4f_{7/2}$ peak, whose binding energy is 84.0 eV.

2.2 Chemical Analysis by XPS

2.2.1 Qualitative analysis

Initial identification of elements present within the sampling depth is achieved by a low-resolution survey scan, measured over a binding energy range of up to 1000 eV. An example of such an XPS survey spectrum is illustrated in Figure 2.8; this has been measured from a phosphate coating on aluminum alloy substrate by exciting with Mg Kα radiation.

A series of peaks are observed on a background which increases to high binding energy (low kinetic energy). By comparing binding energies of the peaks with reference data [51], individual peaks may be identified. Several peaks can often be recognized for each element. For instance, Al2s and Al2p peaks can be seen in the figure. They are due to electron emission from the different subshells. For Zn, the increased spin-orbit interaction yields the $Zn2p_{1/2}$ and $Zn2p_{3/2}$ doublet, where the subscripts identify the possible j values. Such spectra typically show a stair-step appearance associated with each main peak having increased background on the high binding energy side, associated with contributions from the inelastically scattered photoelectrons.

XPS can provide information about chemical state or bonding situation for atoms in a surface region by analyzing high-resolution spectra for a particular photoelectron line. Siegbahn et al [52] first identified the chemical shift effect in XPS, whereby the actual binding energy measured for a photoelectron is dependent to some degree on the actual chemical environment experienced by that electron in the solid. Figure 2.9 shows such an Al2p spectrum from a phosphated aluminum alloy surface. Two peaks are apparent at higher resolution. One at around 75.8 eV is assigned to Al in the oxide form, whereas that at around 72.6 eV results from Al metal. This trend fits expectation from the partial positive charge on the Al which is bonded to O.

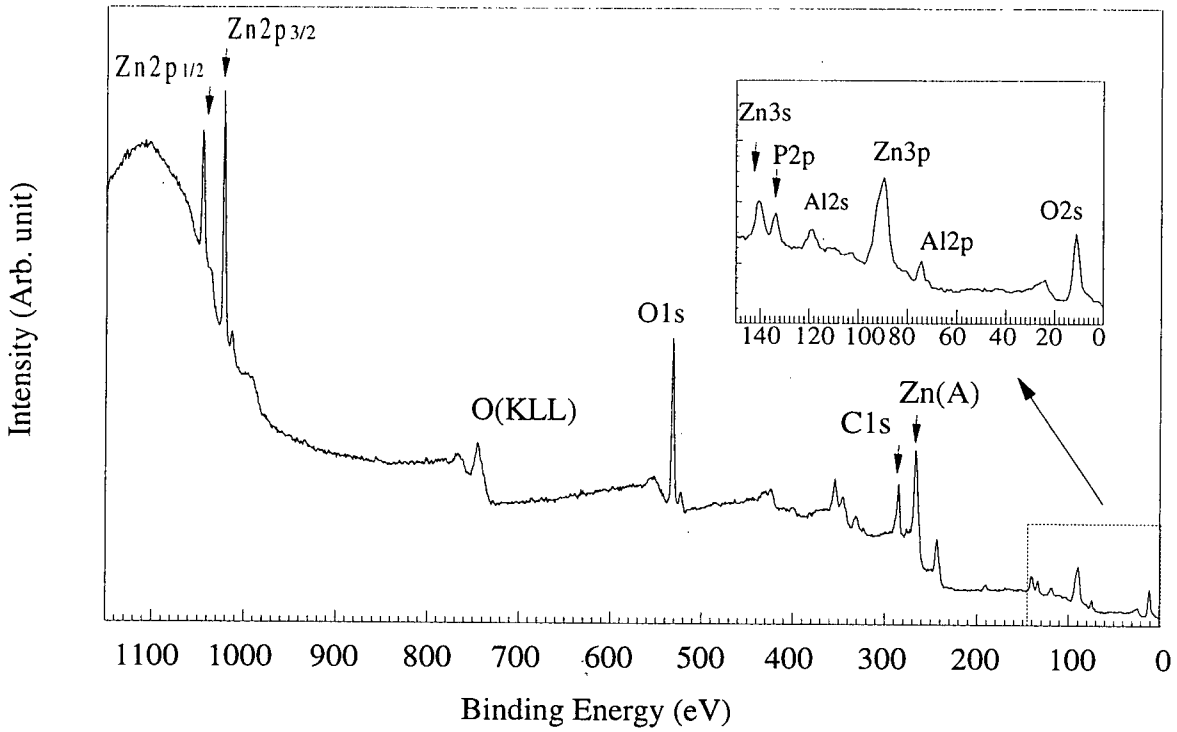

Figure 2.8 XPS survey spectrum of a phosphate coated aluminum alloy

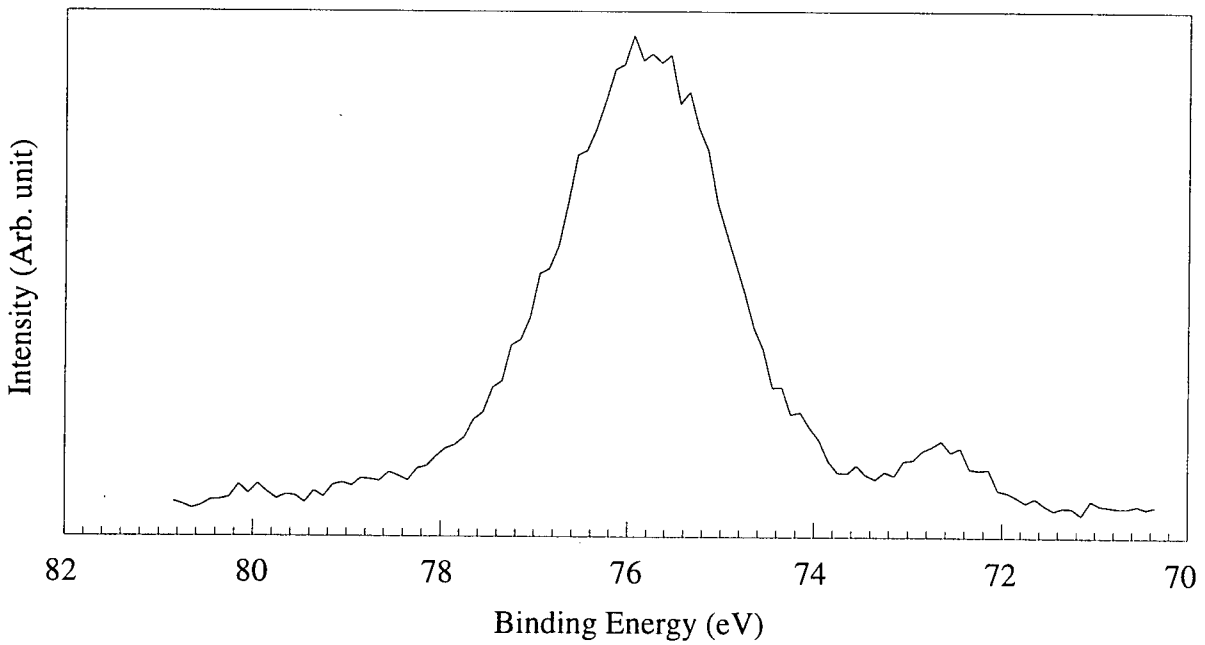

Figure 2.9 Al2p high resolution scan of an aluminum alloy surface

2.2.2 Quantitative analysis

The intensity of a photoelectron peak is generally taken to be proportional to the area of the peak determined after correcting for the effect of the inelastically scattered electrons in the background. The number of elastically scattered photoelectrons collected by the analyzer per unit time depends on the X-ray flux (F), the photoelectron cross section (σ), the number of relevant atoms per unit volume (D), the area of the sample from which the photoelectrons are collected (A), the instrumental detection efficiency (T) and the inelastic mean free path (λ). The contribution to the intensity from an incremental thickness dx in the sample at depth x below the surface (Figure 2.10) is:

$$dI = f\sigma DAT\exp(-x/\lambda)dx \tag{2.5}$$

Simple integration from x = 0 to x = ∞ for a semi-infinite homogeneous sample then gives:

$$I = \int_0^\infty f\sigma DAT\exp(-x/\lambda)dx = f\sigma DAT\lambda \tag{2.6}$$

A commonly used approach for comparing relative compositions of two elements in a sample is to group the instrumental factors f, A, T, as well as σ (for each particular photoelectron peak), into a sensitivity factor S. Such factors, expressed relative to the F1s peak, are available for the MAX200 spectrometer where the transmission function from the manufacturer corrects for the particular instrumental conditions used for each measurement [53]. Then the composition ratio for two elements in a sample can be expressed as:

$$\frac{D_1}{D_2} = \left(\frac{I_1 / S_1}{I_2 / S_2}\right)\left(\frac{\lambda_1}{\lambda_2}\right) \tag{2.7}$$

In principle, one can use tabulated values of λ_1 and λ_2 for the appropriate photoelectrons in the material of interest. For semiquantitative work, a common practice is to take the ratio of λ_1/λ_2 as effectively constant so that the ratio I_1/I_2, from the measured peak intensities, can

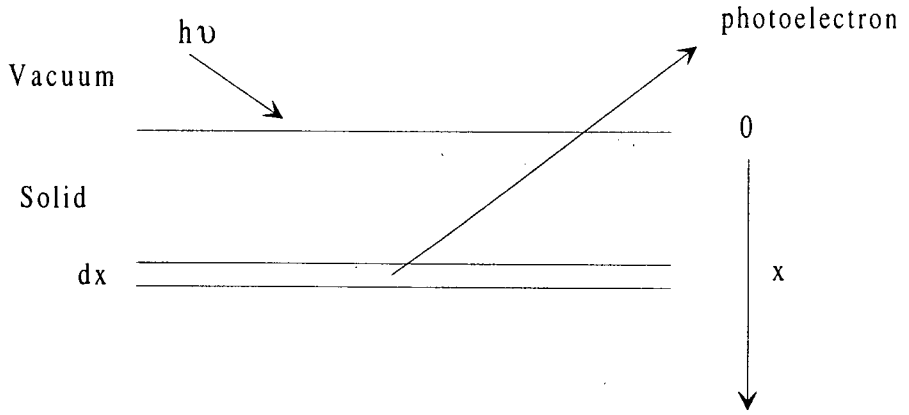

Figure 2.10 Some notation for a semi-infinite homogeneous sample.

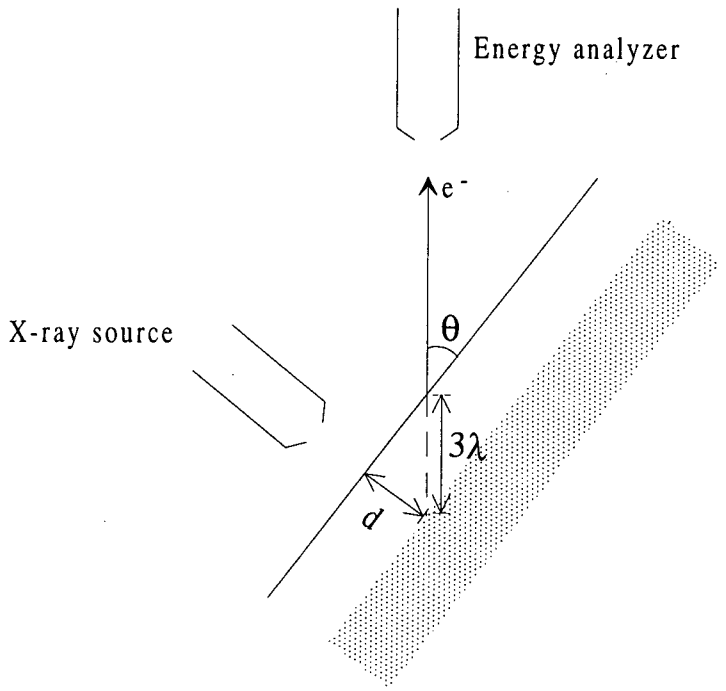

Figure 2.11 Illustration of the principle of angle dependent XPS

help estimate the elemental composition ratio D_1/D_2 within the depth probed.

Before integration of peak area for quantitative analysis, a spectrum must be background subtracted for this energy range. A non-linear approach proposed by Shirley [54] is used in this work. This method assumes that in a photoelectron peak, which dominantly involves elastically scattered electrons, there are contributions from inelastic processes, and that at any part of the spectral peak, the number of inelastically scattered electrons is proportional to the number of elastically scattered electrons at higher kinetic energies. The MAX200 data system will apply the background subtraction program once the appropriate energy range has been chosen by the operator [53].

2.2.3 Angle dependent XPS and bias technique

The surface sensitivity of XPS can be enhanced by varying the take-off angle θ, which is defined as the angle between the surface of a material and the axis of the energy analyzer (Figure 2.11). If θ is below 90° (the normal take-off direction), the sampling depth in effect reduces to $3\lambda\sin\theta$, thereby increasing the surface sensitivity. Varying the take-off angle from a particular sample gives information from different layers near the surface, and thus an indication of the distribution of elements with depth can be derived.

In a practical situation, a sample may consist of an overlayer (thickness d) on top of a substrate material. In relation to measurements associated with varying take-off angle, Equation (2.5), after correcting for angular effects, integrates to yield:

$$I_s = f\sigma_s D_s A T \lambda_s \exp(-d/\lambda_{so}\sin\theta) \tag{2.8}$$

$$I_o = f\sigma_o D_o A T \lambda_o [1 - \exp(-d/\lambda_o \sin\theta)] \tag{2.9}$$

for photoelectron intensities from the substrate and overlayer respectively. In Equations (2.8) and (2.9), λ_s and λ_o are inelastic mean free paths for photoelectrons originating in, and traveling in, the substrate and overlayer respectively, while λ_{so} is the inelastic mean free path of photoelectrons from the substrate traveling in the overlayer. The ratio I_o/I_s increases strongly as θ decreases, and Equations (2.8) and (2.9) can be useful in interpreting the relative orientation or composition gradients for different species for the assumed model [55].

With non-conducting samples, or samples containing insulating regions, care is needed in relation to possible charging effects, arising from a build-up of positive charge because of the loss of electrons in the photo-emission process. This positive charge produces a retarding field in front of the sample such that the photoelectrons have a kinetic energy E_k lower than that predicted by equation (2.1). Conducting samples in electrical contact with the spectrometer do not exhibit charging effects, and even for less conducting samples studied in spectrometers using an unmonochromatized X-ray source, any charge build up is generally neutralized by the background of low-energy electrons produced by Bremsstrahlung radiation. If this neutralization is not complete, some differential charging may occur resulting in broadened and/or distorted peaks [56]. This can complicate XPS data interpretation, although a common practice is to use a low-energy (<10 eV) electron flood gun to minimize or even eliminate this phenomenon [57]. Although differential charging is generally regarded as an unwanted phenomenon, and caution must be exercised in interpreting additional peaks or broadened peaks, the study conducted by Y.L. Leung et al [58], following work by A.J. Pertsin et al [59], indicated that it can be used to advantage in investigating changes in chemical states that may result from such changes in electrical conductivity. This technique is conducted by applying a substantial, and negative, biasing

potential to the sample holder, making the XPS measurement and then shifting the spectrum back to correct for the effect of the bias voltage. If an overlayer on a metallic substrate remains in good electrical contact with the spectrometer, the spectrum will remain unchanged compared with that measured from the grounded sample. However, if the overlayer is partially insulating, some structure may shift to the higher binding energy side of the regular peak position. Such effects can be especially pronounced in measurements made for low take-off angles [58].

2.3 Scanning electron microscopy

2.3.1 Introduction

The scanning electron microscope (SEM) was first introduced to the commercial market in 1965 [60]. It has proven to be an extremely useful technique, particularly to characterize surface morphology by imaging the secondary electron emission. The use of an electron beam can provide a thousandfold increase in resolving power compared with light. Current SEM instrumentation can resolve detail to approximately 3 nm, but the special advantage of this form of microscopy is that it provides a large depth of field compared with an optical microscope. Consequently SEM provides magnified images (up to 300,000x) with a seemingly three dimensional structure.

For a given accelerating voltage, the geometry of the sample surface relative to the beam has a great influence on the intensity of the emission signal, and gives rise to the contrast seen in electron micrographs. It is the low-energy secondary electrons (10 - 50 eV) that are detected, and since they are strongly absorbed by the sample, they must be produced near the surface of the sample in order to contribute to the image formation. Commonly a

large number of secondary electrons will be detected from an elevated part of the surface, but fewer electrons are detected from depressed regions, so resulting in a darker region on the micrograph.

2.3.2 Instrumentation

A Hitachi S4100 SEM (Figure 2.12) was used for this study; it operates under a vacuum of 10^{-6} mbar, obtained by a diffusion pump backed-up by a rotary pump. The main components of the SEM are illustrated in Figure 2.13. The illuminating system consists of an electron gun and condenser lens assembly to focus the beam on to the sample. The electron gun has three components: a filament, a shield and an anode. The electrons are produced by field emission and accelerated to an energy of about 30 keV. The condenser lens assembly then reduces the electron beam diameter from about 25,000 Å to as low as 30 Å. The maximum lateral resolution in SEM is determined by the diameter of the beam as it strikes the sample.

The electron beam is scanned across the sample by deflection coils, while the detector counts the secondary electrons emitted from each region probed on the surface. The detector has a scintillator and photomultiplier, and the final amplified electron signal may be displayed on the cathode-ray tube (CRT), from which photographs can be made for permanent record.

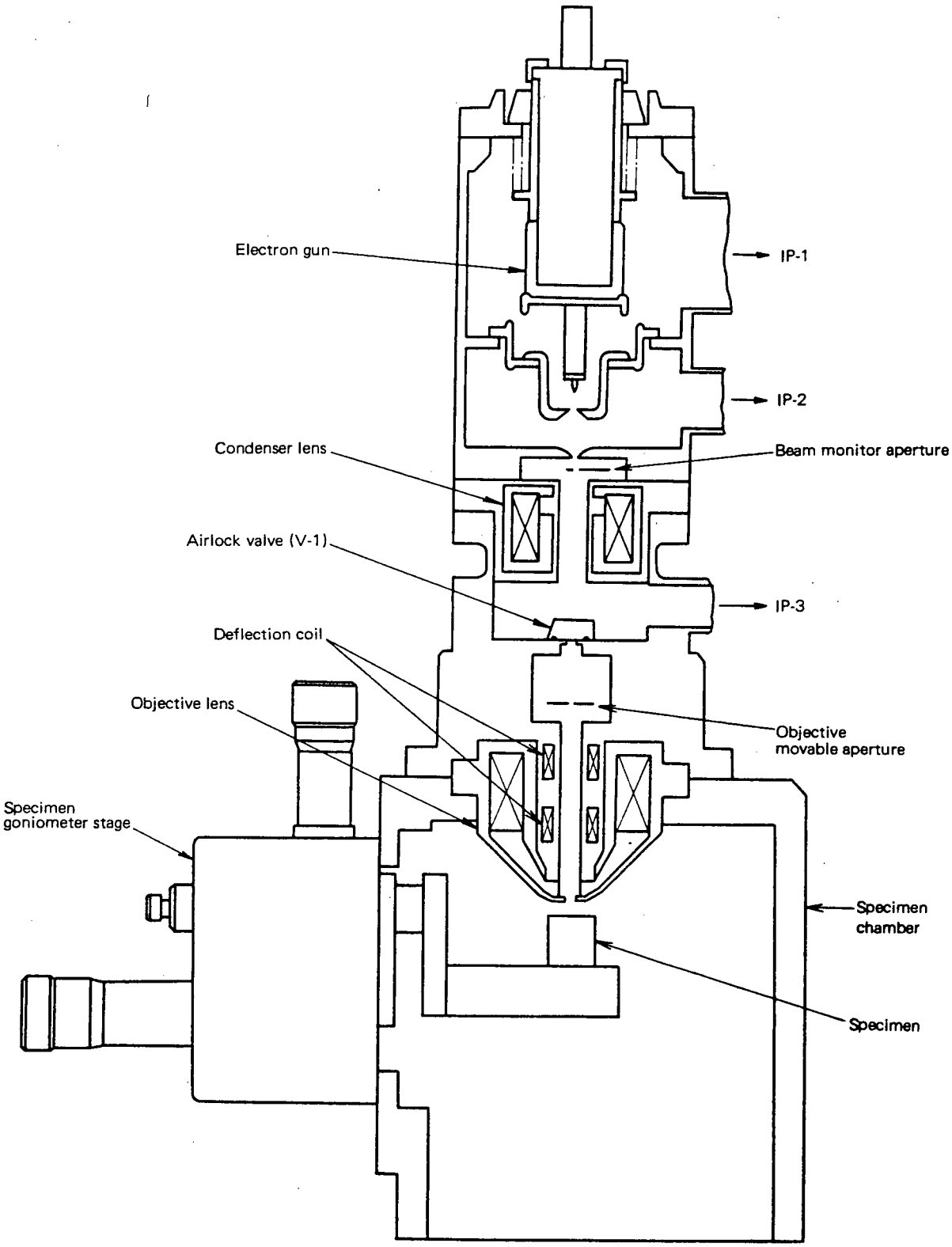

Figure 2.12 Sectional view of S4100 SEM. [94]

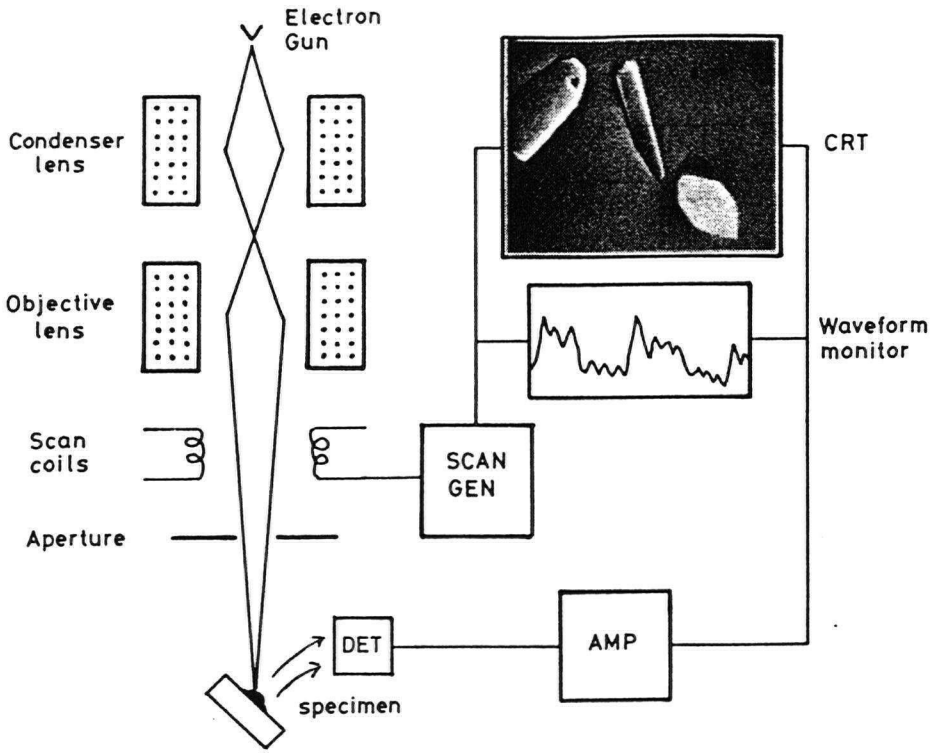

Figure 2.13 Schematic diagram showing the main components of the SEM. [60]

Chapter 3 Phosphating of 7075-T6 Aluminum by Spraying

3.1 Search for a Spraying Method

3.1.1 Sample preparation

Square panels (dimensions 1.0×1.0×0.12 cm) of 7075-T6 aluminum alloy (approximate minority components: 6% Zn, 3% Mg, 2% Cu, 0.5% Fe, 0.4% Si, 0.3% Mn, 0.2% Ti) were prepared. Briefly, these panels were polished with sandpaper and water, then degreased with acetone and methanol in an ultrasonic bath, dried in air, and finally given the Ti-colloid surface conditioning treatment described previously [61]. Two water-based solutions were used for the phosphating processes either by dipping or spraying: solution 1 (each liter contained 16.0 ml of 85% H_3PO_4, 5.36 g ZnO and 0.5 g NaF) and solution 2 (based on composition of 1 but additionally each liter contained accelerators in amounts 1.1 g $KClO_3$ and 0.2 g $NaNO_2$). A specification of the preparation procedure used for each main sample (and its code) studied in this work is included in Table 3.1. Before further study each sample was rinsed with distilled water and air-dried.

3.1.2 Sample characterization

The samples specified in Table 3.1 were characterized by XPS and SEM. Photoelectron spectra were measured with a Leybold MAX200 spectrometer with the pressure of the analysis chamber at 6×10^{-9} mbar and a sampling area of 2×4 mm. The unmonochromatized Mg Kα X-ray source (1253.6 eV) was operated at 10 kV and 20 mA. Survey scans were obtained with the pass energy of the hemispherical analyzer set at 192 eV. The gold $4f_{7/2}$ peak at 84.0 eV was used to calibrate the binding energies reported in this

Table 3.1 Description of samples for phosphating studies

Code in text	Description*
A	7075-T6 aluminum panel wet-polished, followed by degreasing with acetone and then methanol
B	Sample A sprayed with the phosphating solution 1, 85°C, 1 min.
C	Sample A sprayed with the phosphating solution 1, 85°C, 5 min.
D	Sample A sprayed with the phosphating solution 2, 85°C, 1 min.
E	Sample A sprayed with the phosphating solution 2, 85°C, 2 min.
F	Sample A sprayed with the phosphating solution 2, 85°C, 3 min.
G	Sample A sprayed with the phosphating solution 2, 45°C, 1 min.
H	Sample A sprayed with the phosphating solution 2, 65°C, 1 min.
I	Sample A dipped with the phosphating solution 1, 75°C, 5 min.

* Samples B to I were surface pre-conditioned by the Ti-colloid treatment [3.1]

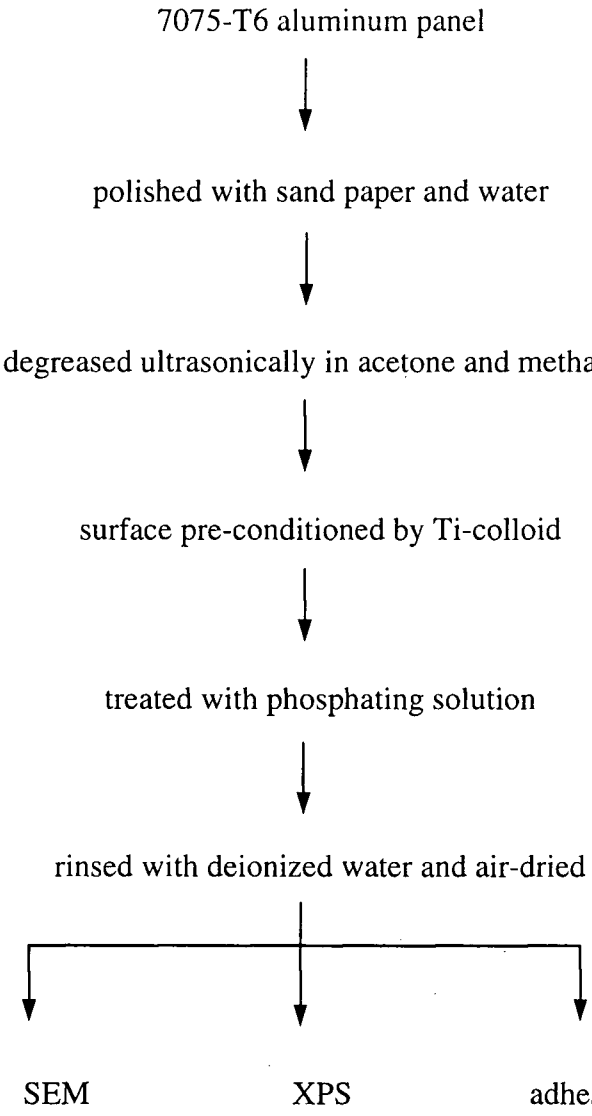

Figure 3.1 A flow chart summarizing the procedures applied to samples which have been subjected to phosphating and subsequent characterizations

thesis. Relative elemental percentages were obtained by integrating corresponding peak areas after making background subtraction and sensitivity factor correction as discussed in Section 2.1.3. Scanning electron micrographs were measured with a Hitachi S4100 scanning electron microscope operated at 30 kV accelerating voltage.

A parallel set of coated and blank samples were tested for their adhesion properties using the arangement indicated schematically in Figure 3.2. For this test, each sample was painted with acrylic primer (Devoe Coatings Co., AMERGUARD 148 W/B), dried in air, and glue (Lepage Ltd., 5 MINUTE EPOXY) was applied to stick the painted side of the sample to a metal holder. After a final air drying for about 2 days, forces perpendicular to the sample surface were applied in opposite directions to the two metal sides until the assembly broke apart. Analysis of the fracture surfaces then identified the region of weakest adhesion for each sample tested.

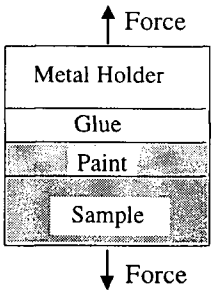

Figure 3.2 Schematic diagram for adhesion test

3.1.3 Results and Discussion

3.1.3.1 Comparison of coatings with and without accelerators

Figure 3.3 shows an XPS survey spectrum for the blank sample A, and it indicates the presence of oxygen, carbon, aluminum and zinc in the surface region. For later reference it is

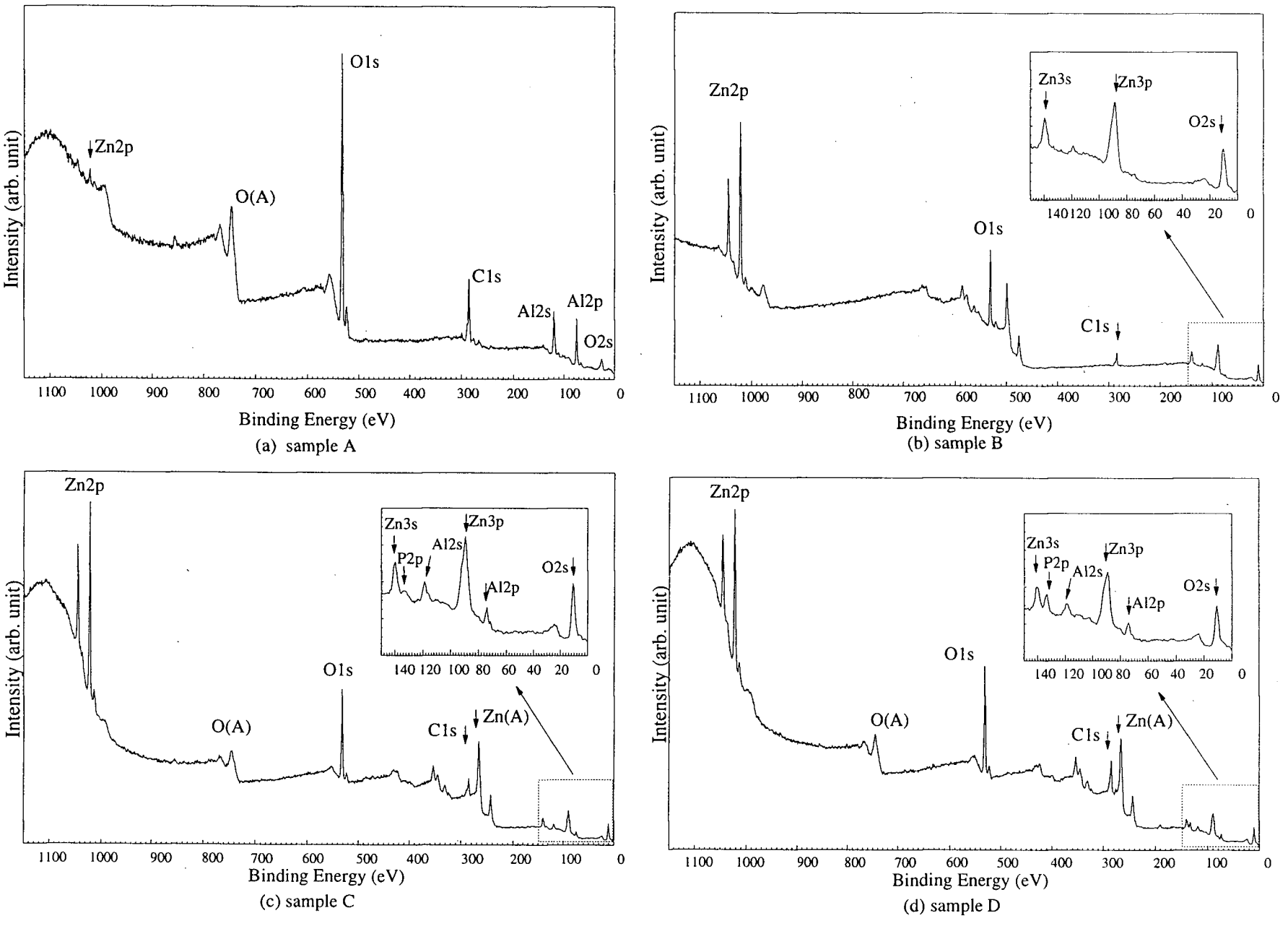

Figure 3.3 XPS survey spectra for samples A, B, C and D

important to note that Zn is present as an intrinsic component of the 7075-T6 aluminum alloy. Some carbon is inevitably present from airborne contamination, and possibly from residual acetone and/or methanol used in the degreasing procedure; similarly the oxygen arises from various sources including metal oxide, residual O-containing organic compounds and airborne contamination. The binding energies for structure in the Al2p spectrum indicates the presence of aluminum in both the oxide (75.8 eV) and metallic (72.6 eV) forms.

The evolution of hydrogen gas acts to slow phosphating reactions [62], and this may have a larger effect with the spraying process, compared with dipping, since the former coatings should be formed relatively quickly. Accordingly, although accelerators were not included in previous work from this laboratory [63, 64], they do need to be considered now. In this section, three specific samples are compared, namely B, C and D (Table 3.1); the first two involve spraying with the phosphating solution 1 (contains no accelerators), but for different treatment times, while the third is for solution 2 (with the $KClO_3$ and $NaNO_2$ accelerators). The XPS survey spectrum from sample B does not detect Al (because of coating film thickness), but P and Zn are seen. The binding energy of P2p (133.0 eV) is consistent with the presence of P in the +5 oxidation state; this is likely to indicate the PO_4^{3-} ion, although in general there may also be some involvement by the $H_2PO_4^-$ and HPO_4^{2-} ions in the surface region. Such participation would act to reduce the Zn/P ratio below the value 1.5 expected from pure $Zn_3(PO_4)_2$ (which is generally seen as the favored product [62]). But for samples C and D, in addition to P and Zn, Al was also detected. Accordingly in the evaluation of the phosphated surfaces by XPS, the trends in the P/Al and Zn/P ratios were emphasized rather than the absolute values.

(a) sample A

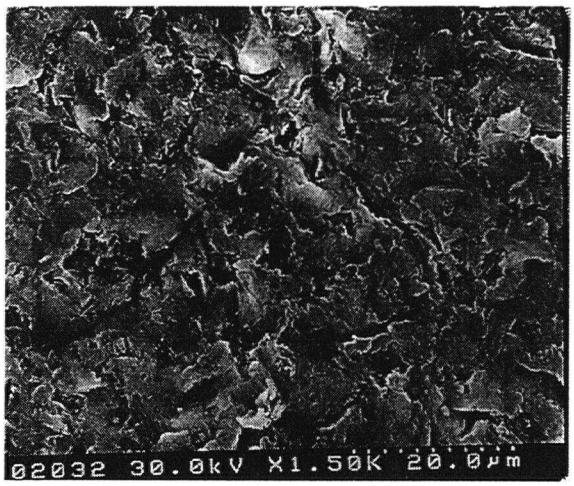

(b) sample C

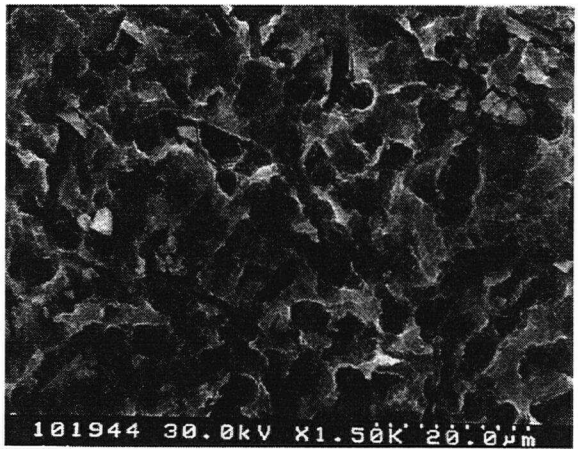

(c) sample D

Figure 3.4 Scanning electron micrographs at x1500 magnification for samples A,C and D

Table 3.2 Relative atomic ratios from XPS for coatings formed by spraying solutions with and without accelerators

Sample	accelerators	P/Al	Zn/P
B	no (soln 1)	no Al detected	25.8
C	no (soln 1)	0.11	9.1
D	yes (soln 2)	0.06	3.8

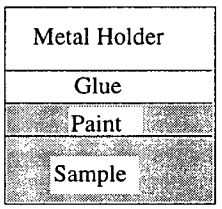

(a) Sample before adhesion test

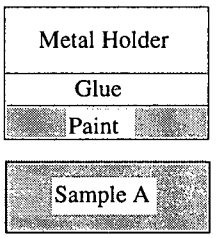

(b) Blank sample after fracture

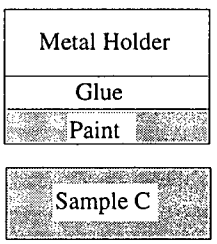

(c) Sample C after fracture

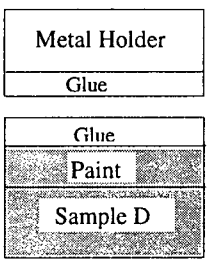

(d) Sample D after fracture

Figure 3.5 Adhesion tests on blank and coated samples

The Zn/P ratio from sample B (25.8) is much larger than that from sample C (9.1), and deviates more from the ratio of pure $Zn_3(PO_4)_2$. Further, since Al is not detected by XPS from sample B, it seems likely that there is a large amount of zinc oxide on the surface. Direct inspection revealed that the surface has a white layer that was easily removed by scotch tape. XPS shows that this de-adhered surface on the scotch tape consists only of Zn and O. It is believed that this zinc oxide results from the bulk alloy component. The coverage of zinc oxide is much less for sample C, accordingly sample C is considered to have a better coating than sample B.

On the other hand, sample D treated with the coating solution 2 containing accelerators has a Zn/P ratio of 3.8, and hence a chemical composition which is closest to that of pure $Zn_3(PO_4)_2$ among these three samples. However, the P/Al ratio of sample D is smaller than that of sample C, suggesting that D has less phosphate in the surface region. As far as chemical composition is concerned, a favorable coating should have both a high P/Al ratio and a Zn/P ratio close to 1.5, but further studies are needed to assess the coatings in samples C and D.

Figure 3.4 compares SEM images (1.5 k magnification) observed from the blank sample A, and from the coated samples C and D. The first shows a rough appearance with a leaf-like structure, the features having a dimension around 8 μm. For sample C, formed by spraying with solution 1 (without accelerators) for 5 min, the coating appears amorphous with some crystalline grains (dimension around 2-3 μm) on top. By contrast, the coating on sample D, formed by spraying with solution 2 (with accelerators) for 1 min, has a crystalline appearance (average dimension 1-2 μm) with the crystal size and distribution quite uniform. Further, the coverage on sample D is much higher than for C. Ideally, small crystal size and

large surface area are desired to allow the paint have better adherence to the substrate. Despite more phosphate in sample C, the coating may be less effective because most of the phosphate is amorphous and this cannot provide as much surface area as an equivalent amount of crystalline phosphate. Further insight is provided by the adhesion tests.

Figure 3.5 summaries the adhesion abilities of the coatings formed with and without accelerators. After fracturing, the breakdown occurs at the point of weakest bonding in the assembly. For the blank sample A, there are three interfaces: namely Al alloy to paint, paint to glue, and glue to Al alloy, but in addition there are bondings within each layer that could in principle fracture. The breakdown of sample A occurs at the paint to Al alloy interface. This strongly suggests that the Al alloy does not have good adhesion to the paint. An improvement is apparent with sample C, insofar as the coated film remains adhered to the metal when the paint-to-coating bond breaks, but this coating still fails to join the alloy tightly to the paint. But with sample D, even though XPS indicates it has less phosphate than sample C (the P/Al ratios are 0.06 and 0.11 respectively), the adhesion breakdown occurs within the glue, showing that there has been a strengthening in the bonding between ZPO coating and the paint. Therefore it appears that the coating in sample D has succeeded in improving the adhesion of the aluminum alloy to the paint, and this represents a first requisite for practical applications. These results suggest that the different performances of the ZPO coatings, formed with and without accelerators, result from their different chemical compositions and structures. Among the three samples studied, sample D, which was treated with accelerators, appears to have the most effective coating.

The above observations show that the accelerators (i.e. $KClO_3$ and $NaNO_2$) have a significant role within the spraying process insofar as they affect the chemical composition,

structure and performance of the ZPO coating. Basically these oxidizing agents react with the H_2 produced from the etching of the metal, and this speeds up both the etching and also the precipitation of phosphate. The more rapid neutralization may result in more active spots for crystallization, so possibly leading to a finer coating. In turn the larger surface area is likely to aid the paint-to-coating adhesion, even though the total amount of phosphate can be reduced by the presence of accelerators.

3.1.3.2 Treatment time

The optimum phosphating time for the dipping process has been reported as 5 minutes [64], but this may be different for the spraying process with otherwise similar parameters. Results in Table 3.3 for samples D, E, and F compare the effect of changing the spraying time while other parameters are constant.

The P/Al ratio can be taken as an index of the amount of phosphate in the coating. The coating after one minute of spraying has P/Al equal to 0.06, but for the two-minute treatment the ratio drops to 0.03, and it drops further to 0.01 for the three-minute treatment. A trend seems established, namely that the amount of phosphate in the surface region of the coating reduces with increasing time for spraying. This may also be seen from the Zn/P ratio. According to Lakeman et al. [65], a dissolution-reprecipitation process occurs at the film-solution interface during the coating process. The decreasing P/Al ratio with treatment time probably indicates that the dissolving of phosphate exceeds the reprecipitation rate for the longer spraying times. This suggests that the dissolving of phosphate has a dominating influence in the spraying process.

Table 3.3 Relative atomic ratios from XPS for samples formed by spraying for different times

Sample	treatment time	P/Al	Zn/P
D	1 min	0.06	3.8
E	2 min	0.03	13.3
F	3 min	0.01	17.7

Table 3.4 Relative atomic ratios from XPS for samples formed by spraying at different temperatures

Sample	spraying temperature	P/Al	Zn/P
G	45°C	0	*
H	65°C	0.06	6.2
D	85°C	0.06	3.8

* No P detected.

Table 3.5 Relative atomic ratios from XPS for coatings formed by different physical methods.

Sample	coating method	P/Al	Zn/P
C	spraying	0.11	9.1
I	dipping	0.18	2.5

3.1.3.3 Treatment temperature

Previous work from this laboratory indicated that phosphating by dipping worked best at around 65 to 75°C [63, 64]. Accordingly this range, including temperatures a bit above and below, was emphasized in the investigation for the spraying process. For the latter, the phosphating solution was held at the designated temperature before spraying, but some small temperature drop may occur during the application. The comparison here emphasizes the samples G, H and D for which the treatment temperatures are 45, 65 and 85°C respectively, while all other parameters are held fixed (Table 3.4).

For spraying at 45°C, essentially no P was detected from the surface region of the coating, but at 65°C and 85°C, Zn, P and Al were detectable. Both samples H and D have more Zn compared with expectation for pure ZPO (Zn/P=1.5). This enhancement is believed to be contributed during the etching process by the presence of zinc in the original alloy. Although samples H and D have the same P/Al ratios, D has less Zn according to Zn/P ratio. It is concluded that sample D has more ZPO and less zinc oxide than sample H. This suggests the views that sample D has a better coating, and that the spraying process is favored by temperature of 85°C compared with the others considered.

Because sample D is the best among samples formed from different coating solutions (Section 3.1.3.1) and for spraying for different times (Section 3.1.3.2), it is concluded that the treatment conditions for forming sample D (85°C, 1 min. with accelerators) gives the most favorable coating among tests made so far.

3.1.3.4 Comparison of dipping and spraying processes

Dipping and spraying are two different methods to apply coating solutions to solid surfaces. With dipping a sample is simply immersed into the coating solution, while with spraying the solution is pressure-forced, as evenly as possible, on to the sample surface. In general the two methods of application result in significant differences between the coatings. Since effective ZPO coatings on 7075-T6 aluminum alloy could be obtained from the dipping process using solution 1, which had no accelerators, an exploratory test of the spraying process was first made with this solution. A specific comparison is referred to here between sample C (coating applied by spraying) and I (coating applied by dipping). Both applications were for 5 min, although their temperatures of application were close to optimal for each method of application.

P, Al and Zn were detected from both samples C and I. According to the P/Al ratio, the coating formed by dipping has more phosphate. The lower Zn/P ratio in sample I suggests that it has a smaller amount of zinc than sample C, and also a closer approach to the "ideal" Zn/P ratio of 1.5. This is taken to indicate that the dipping method gives a better zinc phosphate composition than the spraying method.

The coatings from these two methods of application are also contrasted by SEM observations of their morphologies. Both samples show an amorphous coating phase and a crystalline coating phase [64]. The sizes of the individual crystal grains were estimated to be in the range of 0.1-0.5 μm. As mentioned in Section 3.1.3.1, sample C also has these two phases, but the average size of the crystals is much larger (5 μm). Also the coating is less dense, and the coverage lower. The main differences observed here are broadly interpreted in the following.

With dipping, the pH of the metal-solution interfacial region rises due to the dissolution of aluminum by acid; in turn Zn^{2+} and PO_4^{3-} ions precipitate on to the metal surface, so reducing the concentrations of Zn^{2+} and PO_4^{3-} in the interfacial region compared with the bulk solution. Zn^{2+} and PO_4^{3-} ions from the bulk solution will replenish by diffusion, but this process being gradual, and less disturbed, appears to facilitate the slow growth of phosphate crystals, and hence the formation of a better zinc phosphate layer.

By contrast, the spraying process is more disturbing with fresh solution continually impacting on the substrate surface. Moreover, this may suppress the further growth of the initially formed zinc phosphate crystals. In general, coatings obtained by spraying are often thinner than those prepared by dipping. On the other hand, in a spraying process, because the supply of the fresh solution to the interface is instant, the etching rate can be greater than the precipitation rate. As a result, coating conditions are favored by the shorter spraying times.

Overall, coatings obtained by spraying are not as good as those prepared by the dipping method. Nevertheless, with suitable modifications in the composition of the coating solution and working conditions, acceptable coatings can still be achieved, particularly in relation to the adhesion ability of the 7075-T6 alloy to organic paint.

3.2 Effect of Polishing

There have been persistent indications that the details of substrate polishing can significantly affect subsequent coating performance [66] and our earlier tests on the coatings pointed to the advantages of using 1200 grit sandpaper in polishing [67]. However, the emphasis now is to compare the use of two different 1200 grit sandpapers, one composed of aluminum oxide and the other of silicon carbide.

3.2.1 Sample preparation

The sample preparation procedures here are similar to those described in Section 3.1.1, except that only the phosphating solution 2 was used; further polishing was done with 1200 grit silicon carbide sandpaper as well as the aluminum oxide sandpaper. The detailed procedures are summarized in Figure 3.6.

3.2.2 Sample characterization

The above treated samples were evaluated by XPS, SEM and the adhesion test. In XPS, survey spectra were measured as described in Section 3.1.2, while high resolution spectra were made for a pass energy of 48 eV. Some spectra were measured for different values of the take-off angle θ; additionally uses were made of the bias potential technique. For the latter, spectra were obtained by applying a negative bias potential (-94.0 V) to the sample, and then, after measurement, mathematically shifting the energy scale back by 94.0 eV as described in Section 2.2.3. Scanning electron micrographs were measured and adhesion tests conducted as described in Sections 2.3 and 3.1.2 respectively.

3.2.3 Results and discussion

3.2.3.1 Adhesion test

After spraying the ZPO solution 2 on to the blank samples that had been polished with the different sandpapers, adhesion tests were carried out to compare the effectivenesses of these treatments. Results of the adhesion tests on samples A2 and B2 are summarized in Figure 3.7.

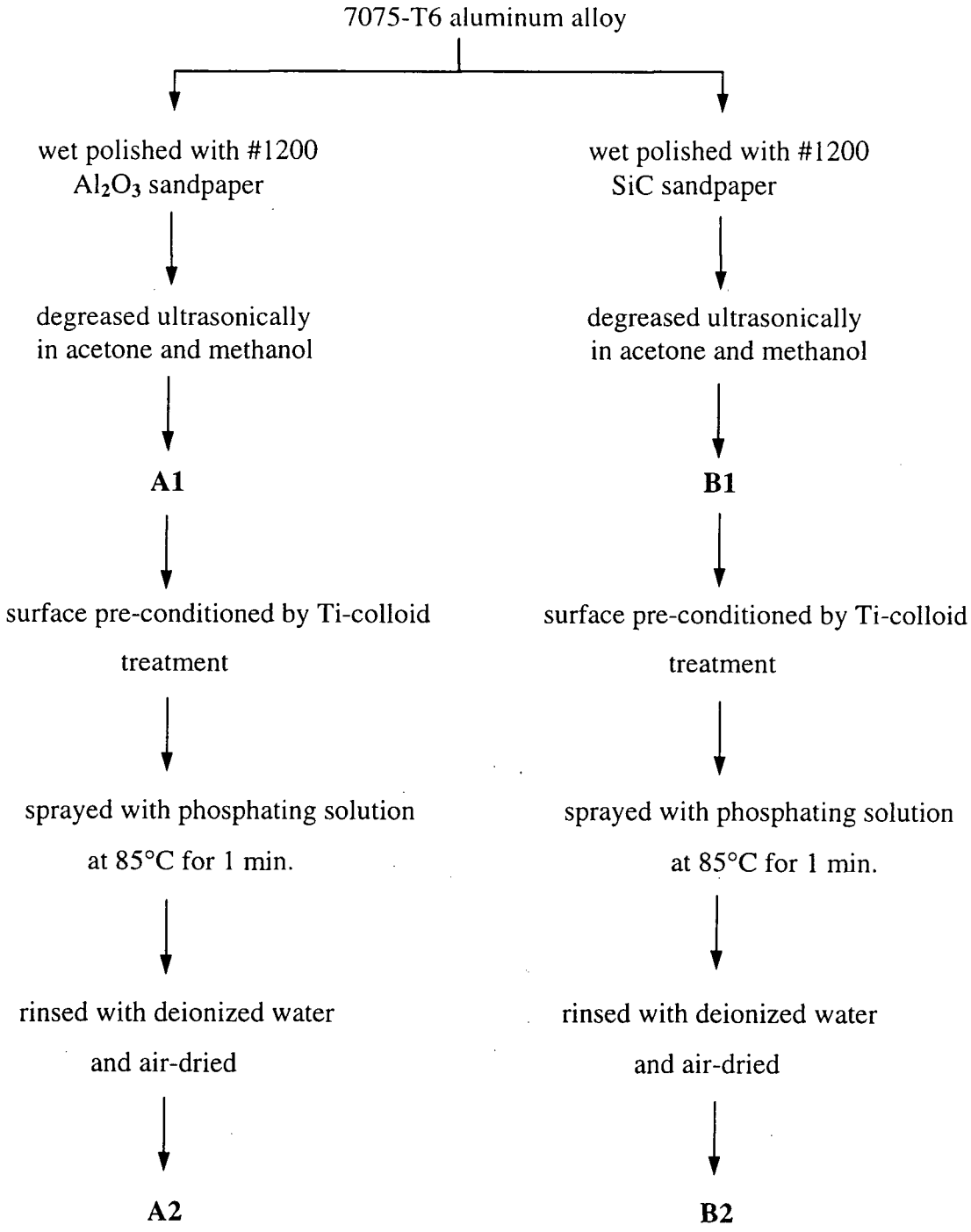

Figure 3.6 A flow chart describing the sample preparation procedures for polishing effect studies

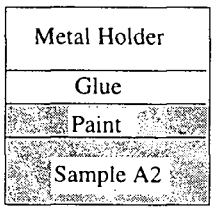

(a) Sample A2 before adhesion test

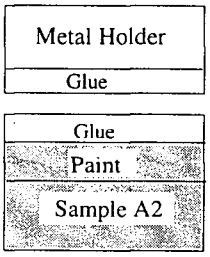

(b) Sample A2 after fracture

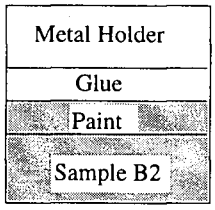

(c) Sample B2 before adhesion test

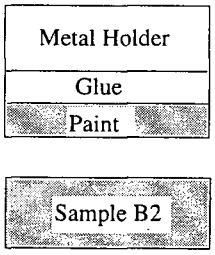

(d) Sample B2 after fracture

Figure 3.7 Adhesion tests on samples A2 and B2

It is noted that the breakdown of sample A2 occurred within the glue layer, which suggests the joining of the Al alloy to the ZPO coating, and the coating to the paint, are not the points of weakest bonding in the assembly. Therefore it can be inferred that the pre-treatment and the phosphating process are able to produce a coating with promising adhesion properties. By contrast, in this context sample B2 fails to produce an effective coating. Figure 3.7 reports that for B2, the breakdown occurred between the substrate and the paint. Since the only difference between the treatments for samples A2 and B2 is in the polishings by different types of sandpaper, it appears that the natures of the sandpapers have had an influence on the subsequent coatings. This point is analyzed further in the following.

3.2.3.2 Characterization by XPS

To evaluate the composition of the polished samples and the samples after a spray coating treatment, XPS measurements were carried out for the four samples designated A1, A2, B1 and B2 (Figures 3.8 and 3.9). Both sample A1 (blank panel polished by Al_2O_3 sandpaper) and sample B1 (blank sample polished by SiC sandpaper) showed essentially identical surface compositions with the elements Al, Zn, O and C being readily detected in both cases. The Zn originates with the 7075-T6 aluminum alloy, but it is worth noting that no Si could be identified in the spectrum of B1. This latter observation supports the view that the differences in adhesion behavior do not originate with direct transfer of sandpaper particles to the polished surface.

However, the survey spectra from the phosphated samples A2 and B2 are quite different (Figure 3.9). In addition to the elements detected from the blank samples, after coating P was present in A2, although no P was detectable in the survey spectrum from B2.

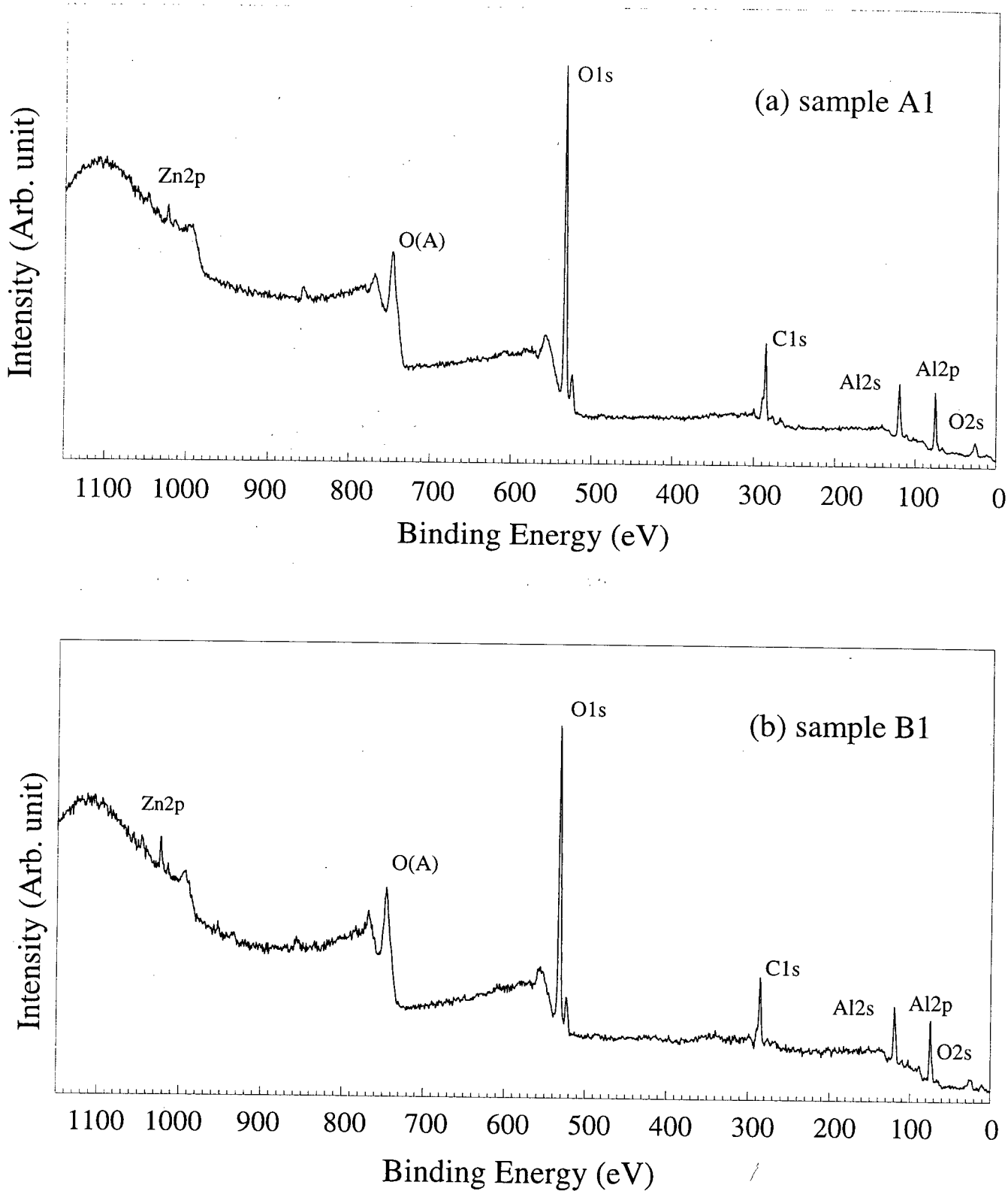

Figure 3.8 XPS survey spectra for samples A1 and B1

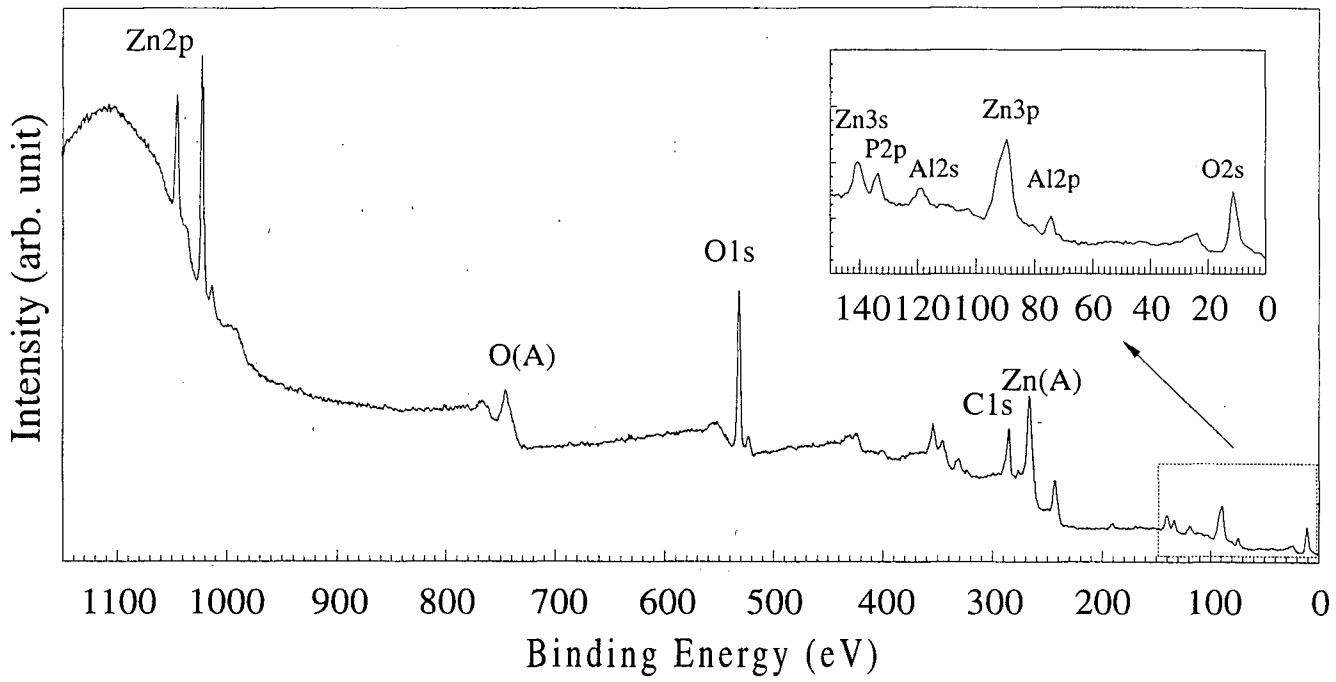

(a) sample A2

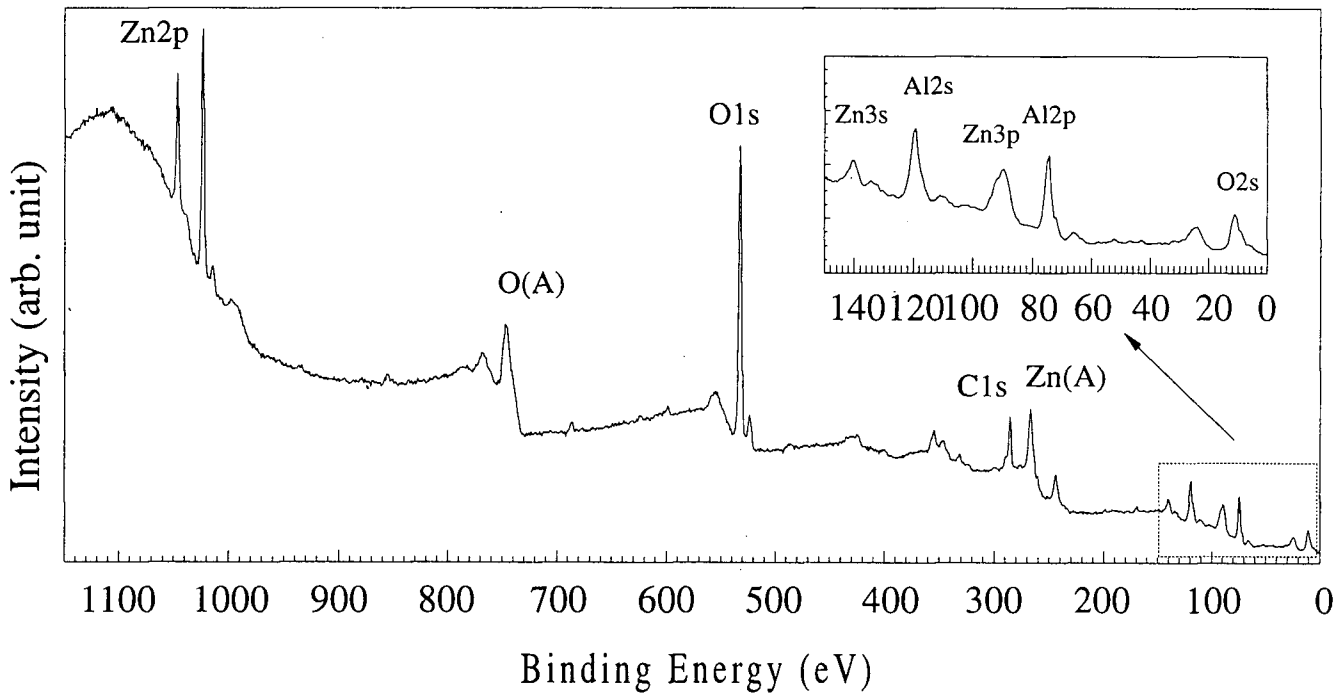

(b) sample B2

Figure 3.9 XPS survey spectra for samples A2 and B2

For the former, the P2p binding energy (133.0 eV) suggests that the P exists as PO_4^{3-}, and therefore that a phosphate coating has been obtained. But overall it is evident that polishing by the silicon carbide sandpaper does not result in a successful formation of phosphate coating, and this presumably gives the reason why sample B2 failed the adhesion test. These results indicate that the composition of sandpaper used in polishing pretreatments, as well as the size of the particles, affects the subsequent phosphate coatings.

But in addition, the narrow-scan Al2p spectra from samples A1 and B1 (Figure 3.10) do indicate difference. Both samples show aluminum in the metallic and oxide forms. However, by contrast, the metallic peak from sample A1 is smaller than that from sample B1. A possible reason is the oxide layer on sample A1 is thicker than that on sample B1, and that the former allows detection of less signal from the metallic form underneath. In addition, the full width at half maximum (FWHM) for the oxide peak from sample A1 (2.2 eV) is larger than that from sample B1 (1.9 eV); this difference may suggest either a greater variety of chemical states in sample A1, or that this sample experiences more surface charging.

For both samples the metallic peaks in the Al2p spectra are at 72.6 eV, but for sample B1, the oxide peak is at 75.4 eV, while for sample A1 the oxide peak has shifted to 75.8 eV. This is about 0.4 eV higher than the standard value [68]. It appears likely that some charging occurs in B1 either due to the thicker oxide layer, or due to some Al_2O_3 being transported from the sandpaper to the sample surface during polishing.

To further investigate the difference between the Al_2O_3 polished surface and the SiC polished surface, the bias potential technique was applied to measurements of the Al2p narrow-scan spectra. Figure 3.11 shows that A1 and B1 have different results. For sample B1, after correcting for the effect of the bias potential, both the metallic and oxide peaks

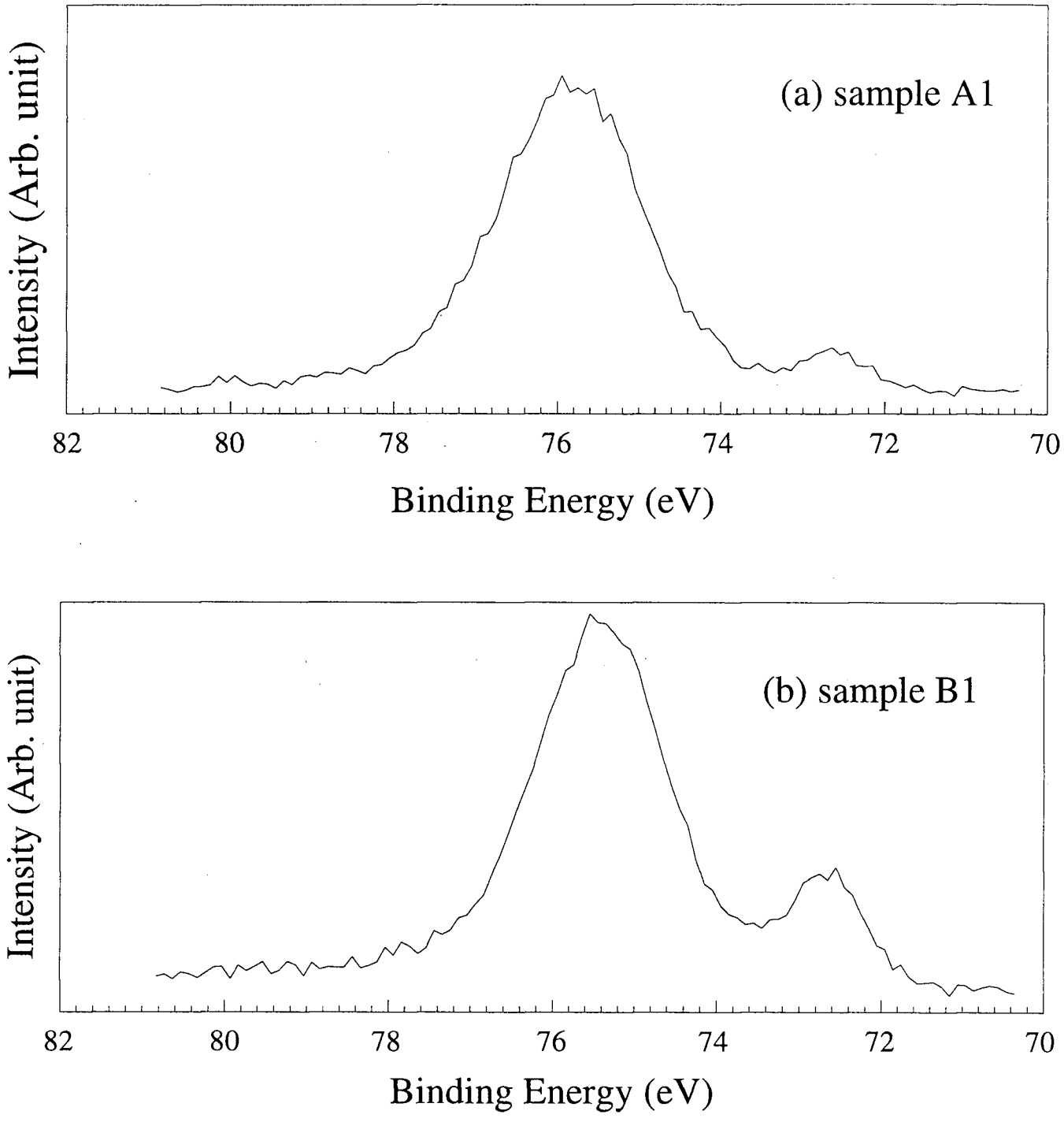

Figure 3.10 Al2p narrow scan spectra for samples A1 and B1 at normal take-off angle

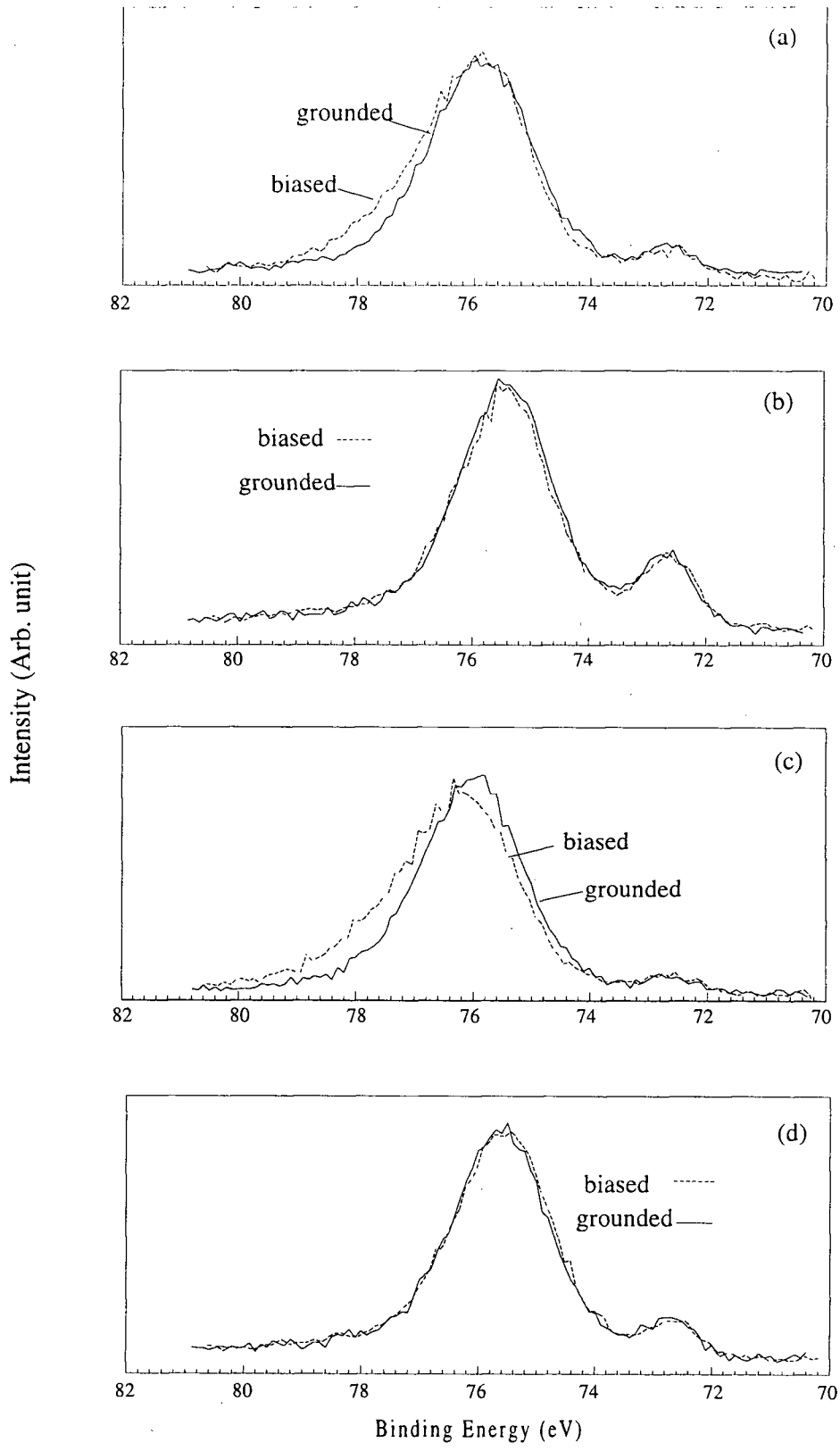

Figure 3.11 Comparison of Al2p spectra measured with bias potential technique at different take-off angles:
(a) sample A1, take-off angle 90°; (b) sample B1, take-off angle 90°
(c) sample A1, take-off angle 30°; (d) sample B1, take-off angle 30°

recover their positions observed in the unbiased spectra. This implies that the oxide layer is in good electrical contact with the metal. But for sample A1, the application of the bias potential affects the oxide peak (not the metallic peak), and this is most obvious for θ=30° (Figure 3.11 (c) and (d)). These observations support the view that in A1 some part of the aluminum oxide is not in good electrical contact with the metal. This "loosely-bonded" aluminum oxide layer is presumably produced by the interaction of the aluminum oxide sandpaper during the polishing treatment, although it may involve some insertion of particles directly from the sandpaper. No such effect is observed for sample B1, but the difference in the nature of the surface layer with polishing by silicon carbide sandpaper appears not to favor the subsequent formation of a phosphate coating by the spraying method.

3.2.3.3 Analysis by SEM

To examine the polished surfaces more closely, SEM micrographs were taken for samples A1 and B1 at 1.5 k magnification (Figure 3.12). It can be seen that A1 has a much rougher surface with layers of leaf-like structure. These "leaves" appear loosely bonded to each other, but the structure seems to be part of the original aluminum oxide rather than having been introduced from the sandpaper. It is hypothesized that this structure gives the poorer electrical contact with the metal, but that it also provides a favorable base for the subsequent phosphating. By contrast, the surface of B1 is smoother, with a lack of wrinkles, and while this bonds more tightly to the layer below, it apparently does not provide enough phosphating sites to form a well-adhered coating.

3.3 Concluding remarks and future work

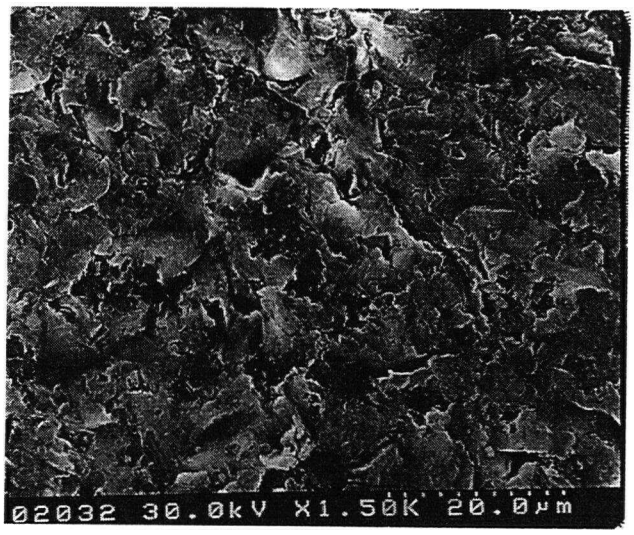

(a) sample A1

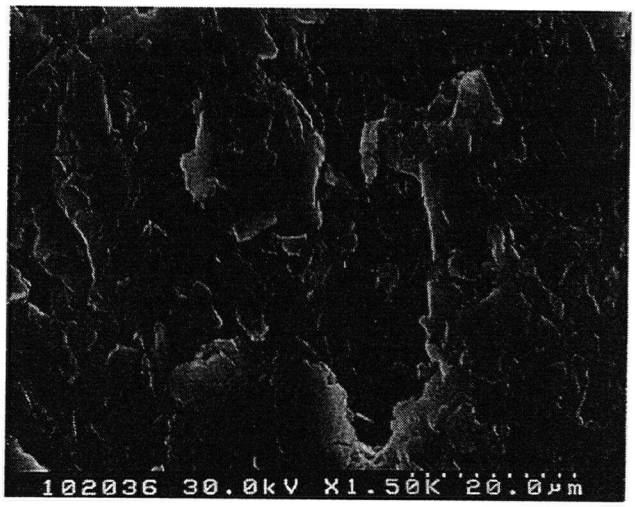

(b) sample B1

Figure 3.12 Scanning electron micrographs at x1500 magnification for samples A1 and B1

3.3.1 Concluding remarks

The research reported in this Chapter has given an initial view of using a spraying method for phosphating 7075-T6 aluminum alloy. The objective was to gain some new information on how the quality of the coating was affected by such factors as accelerators in the coating solution, treatment time and treatment temperature. XPS studies indicate that the coated sample consists of a mixture of zinc phosphate, zinc oxide and aluminum oxide. Elevated temperature (85°C) and short treatment time (1 min) plus the added accelerators ($KClO_3$ and $NaNO_2$) are found favorable to the formation of an effective coating, for which SEM micrographs indicate a morphology of evenly distributed fine crystals with dimension about 1-2 μm. Further, adhesion tests show that this coating has good adhesion to both the metallic substrate and the applied paint. It is hoped that with such a conversion coating, paint will bond better to aluminum alloy resulting in improved corrosion resistance for the products.

That conditions for successful coating can be quite subtle is suggested by the observation that the type of sandpaper used in polishing plays an important role in the phosphating of 7075-T6 aluminum alloy. For example, the zinc phosphate coating formed on a surface polished by 1200 grit aluminum oxide sandpaper had good adhesion to paint, whereas polishing by 1200 grit silicon carbide sandpaper failed to result in an effective phosphate coating. In both cases, aluminum oxide was found on the polished surfaces. But for the surface polished by Al_2O_3 sandpaper, the topmost oxide layer is loosely-bonded and not in good electrical contact with the metal, while for the SiC polished surface, all the aluminum oxide layer is in good electrical contact with the metal. Thereby it is believed that

the presence of the loosely-bonded oxide aids possibilities for the successful phosphate coating.

3.3.2 Future work

Future research is possible in several directions:

(1) Corrosion resistance studies

Since one of the major goals of applying phosphate coatings is to improve the corrosion resistance of the aluminum alloy, further studies on the corrosion resistance of the phosphate coating itself and that after being painted will be of great interest.

(2) Improvement of the coating process and coating performance

From our SEM studies, it can be seen that the coverage of our best coating from spraying is not as high as that from a dipping process. It is believed that if the coverage could be improved, and the crystal size reduced, the phosphate coating would have more surface area for bonding with paints and therefore have a better adhesion ability.

The solution temperature required for our spraying process at present is 85°C. If this could be lowered to moderate temperature (40 - 60°C), or even to room temperature, which has been realized for some phosphating processes by dipping [69,70], there would be big advantages (e.g. easier to handle, less energy consumption). Such improvements would require adjustment in the composition of the phosphating solution.

(3) Phosphating of other aluminum alloys and other metals

While our research focused on 7075-T6 aluminum alloy, the conclusions drawn from this study may also apply to the phosphating of other aluminum alloys, and indeed other

metals. Such further studies should help the development of the mechanistic principles underlying these coating processes.

(4) Studies on other non-chromium conversion coatings

Like phosphate coatings, some organic conversion coatings, for example organosilanes and organophosphonates, may also improve the adhesion between metals and paints [71, 72], and thereby contribute to an improvement in the corrosion resistance of metals. These organic compounds have a functional group at one end that can bond to paint, and a hydrolysable functional group at the other end that can form chemical bonds with the metallic substrate. Since such organic materials can be applied much easier than is the case with phosphating, these coatings could be competitors to phosphate coatings in the future. An aspect of this is considered further in the next Chapter.

Chapter 4 Characterization of a Silane/Aluminum Interface

4.1 Introduction

One approach to the protection of aluminum and its alloys against corrosion is to apply an organic (polymer) coating. However, due to their completely different properties, the bond between the polymer and the metal is not generally strong enough to resist either mechanical stress or chemical attack from aggressive species in the environment. As a consequence, adhesion promoters or coupling agents are frequently applied. Among such agents are silanes with general structural formula X_3SiY, where X is a hydrolysable group and Y is an organofunctional group capable of reaction with the polymeric binder. Some commercially available silane adhesion promoters are given in Table 4.1. The bonding mechanisms by which silanes improve the adhesion between organic polymers and inorganic substrates is not fully understood, although several theories have been proposed [73]. A widely accepted theory holds that the silanes hydrolytically form direct chemical bonds between polymer and substrate [71]. It is generally accepted that silanes hydrolyze stepwise in water to give the corresponding silanols [74], and these may hydrogen bond to one another, and condense to form siloxane polymers [75] (Figure 4.1). Likewise on metal surfaces, usually containing some oxide, water can adsorb as hydroxyl group (M-OH), or as molecular water hydrogen bonded to the surface [76], and in combination, water may eliminate with formation of a direct M-O-Si covalent linkage.

The molecular structure of films formed by γ-APS on iron substrates has been studied by Boerio and Williams using reflection-absorption infrared spectroscopy and XPS [75] An intense band near 1135 cm^{-1} was assigned to an Si-O-Si asymmetric stretching mode. No

(a) Hydrolysis

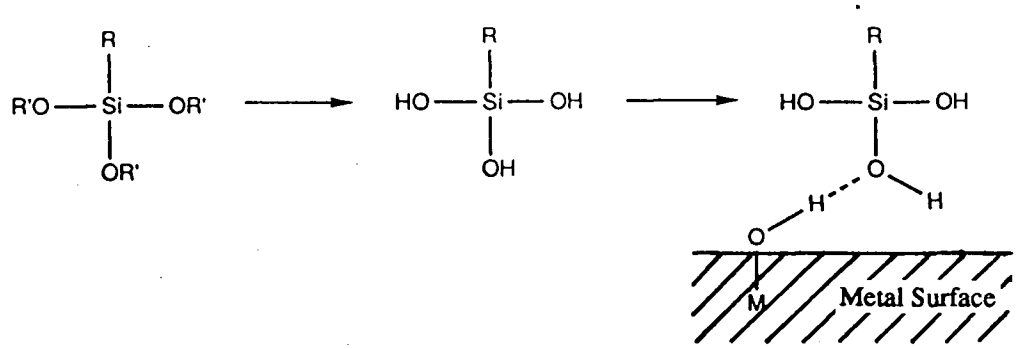

(b) Hydrogen Bonding

During Evaporation

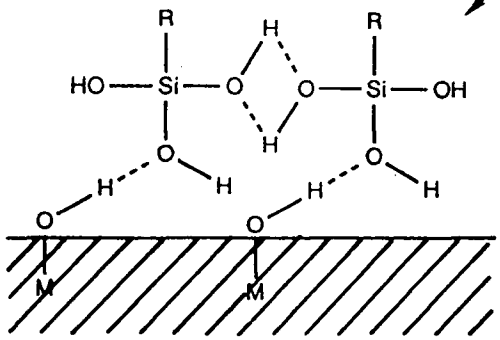

During Drying

(c) Polymerization

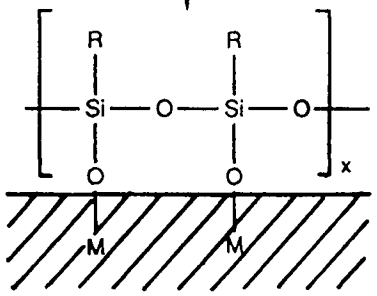

Figure 4.1 Deposition of silane on metal surface

evidence was presented for the existence of direct Al-O-Si bonding. Sung et al. [77] studied the natures of silane films on glass and metals by Fourier transform infrared spectroscopy and concluded that the silane films corresponded to polysiloxane networks. Although early studies provided indirect evidence [78 - 82], evidence for the existence of direct covalent bonds between silane and metal is limited, other than that presented by Gettings and Kinloch [83]. These authors used secondary ion mass spectrometry (SIMS) , and detected an ion of mass 100, assigned as $FeSiO^+$, in the spectrum after a steel surface had been treated with γ-GPS. They considered this as strong evidence for the formation of direct Fe-O-Si chemical bonds between the metal oxide and polysiloxane primer.

Earlier work in our laboratory suggested that angle-dependent X-ray photoelectron spectroscopy (ADXPS), in combination with a bias potential technique, may give a new way for probing the interfacial bonding between oxidized aluminum and silanes, and for aiding the identification of relationships between atomic-level interfacial structure and macroscopic properties [84, 85]. For a thin layer of γ-glycidoxypropyltrimethoxysilane (γ-GPS) deposited on chemically etched aluminum, it was hypothesized that new structure apparent in Al2p spectra for small exit angles in ADXPS, after applying a negative biasing potential, may indicate a "chemical shift" effect associated with the Si-O-Al bonding [85]. The evidence was indirect; it depended on the existence for some silane-aluminum systems of this additional structure in Al2p spectra, induced by differential charging, and an associated correlation with corrosion protection. The present research reports further observations on the same system, and includes an attempt at characterizing the interfacial bonding with static SIMS [86].

Table 4.1 Representative commercial silanes

Abbreviation	Chemical structure	Organofunctional group
VS	$CH_2=CHSi(OCH_3)_3$	Vinyl
CPS	$ClCH_2CH_2CH_2Si(OCH_3)_3$	Chloropropyl
γ-GPS	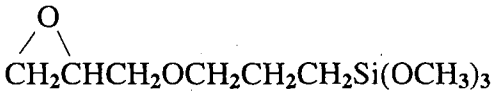	Epoxy
MPS	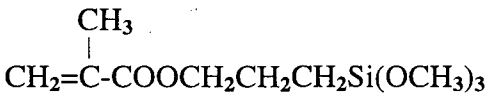	Methacrylate
APS	$H_2NCH_2CH_2CH_2Si(OC_2H_5)_3$	Primary amine
AEAPS	$H_2NCH_2CH_2NHCH_2CH_2CH_2Si(OCH_3)$	Diamine
MGPS	$HSCH_2CH_2CH_2Si(OCH_3)_3$	Mercapto

4.2 Secondary ion mass spectrometry (SIMS)

4.2.1 Introduction

Over the past twenty years secondary ion mass spectrometry (SIMS) has developed into a powerful technique for studying the chemical composition and structure of solid surfaces [87]. It is also a complementary technique to the other methods like X-ray photoelectron spectroscopy and Auger electron spectroscopy. SIMS involves bombarding a surface with primary ions of known mass, charge and energy, and detecting secondary positive and negative ions after they have passed through a mass analyzer. The SIMS sputtering process is illustrated in Figure 4.2. An incident ion beam (energy 0.5 - 30 keV) impacts with the sample surface, from which material is sputtered into vacuum. These fragments can consist of one or more atoms; most are neutral but a few percent carry either positive or negative charge. These ions are collected by a mass spectrometer which measures the mass/electric charge (m/z) ratio [88].

SIMS is a microanalytical technique that combines high sensitivity with good elemental selectivity [89]. It can analyze all elements in the periodic table including isotopes (from H to U) with ppm sensitivities for most elements and ppb for a few; also it can indicate local bonding arrangements in the solid from the form of molecular fragments detected among the secondary ions. SIMS is necessarily a destructive technique and hence each analysis should be performed on a new area of the sample. Also the proportion of secondary ions generated during the sputtering process varies greatly between different elements and compounds, and this makes quantitative analysis difficult.

SIMS analyses may be conducted within three regimes, namely static SIMS, dynamic SIMS and imaging SIMS. Static SIMS (SSIMS) uses primary beams with typical current

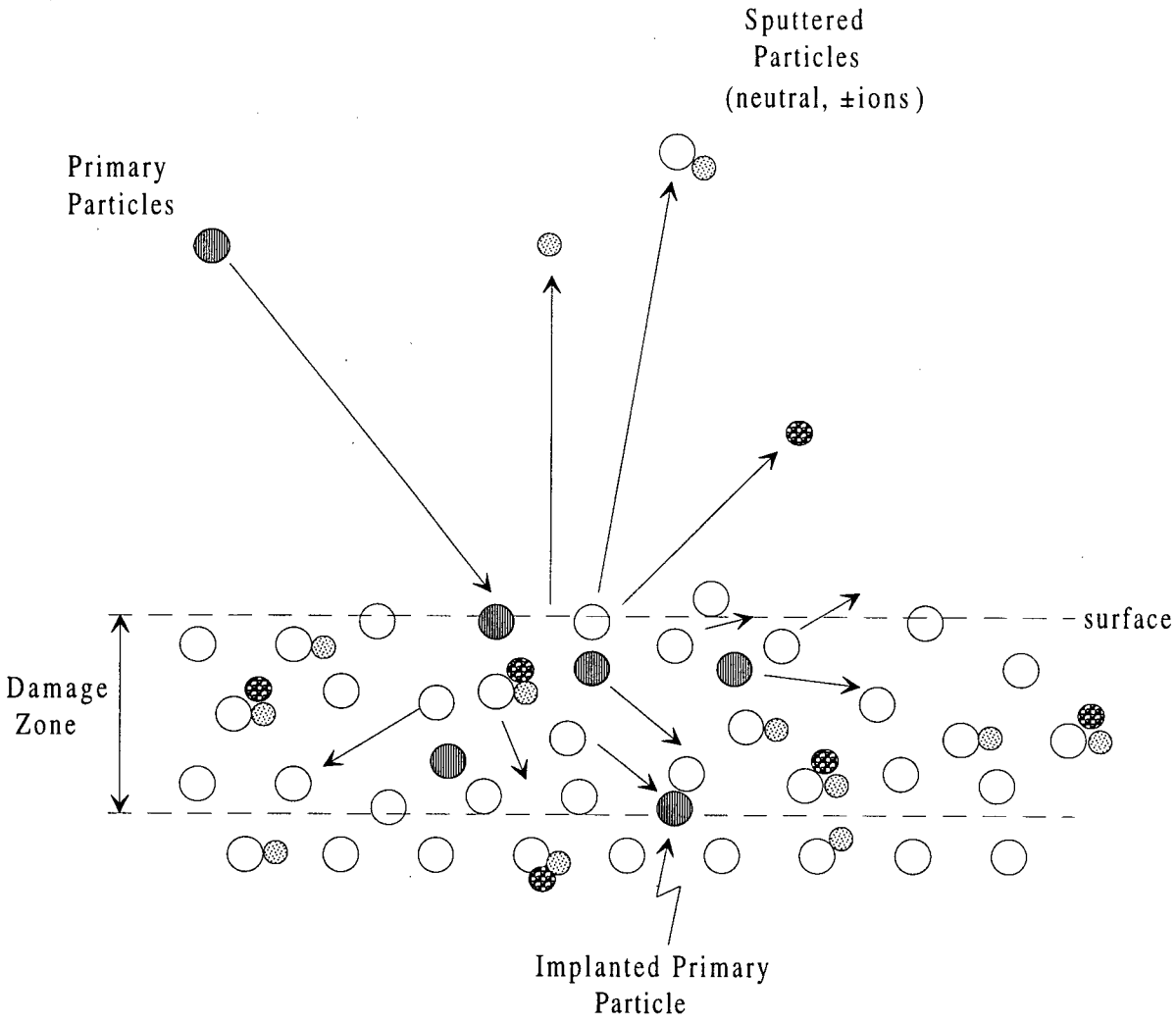

Figure 4.2 Schematic diagram of SIMS sputtering process

densities of around 1 $nAcm^{-2}$ or below [90]. Then every primary ion impacts on a virgin area of the surface, and SSIMS can be used for studying the chemical structure of the topmost layer, as well as its elemental composition.

Dynamic SIMS uses higher flux densities of primary ions to obtain much higher yields of secondary ions. Then a surface can be eroded rapidly, to yield high-sensitivity concentration-depth profiles, but the primary ion doses are large enough to cause significant disruption of the near-surface region of the sample, so losing most molecular information. Consequently dynamic SIMS is used almost exclusively for elemental analysis.

Imaging SIMS uses a microfocused liquid metal ion beam (resolution 50-500 nm) in which metal ions are field ionized from a sharp tungsten tip [91]. By raster scanning the beam over a defined area, and simultaneously collecting the emitted ions, a chemical image can be generated.

4.2.2 Instrumentation

The heart of a secondary ion mass spectrometer is the mass analyzer. The one used in our system is a VG MM12-12S 800 amu quadrupole mass analyzer. It analyzes ion masses by subjecting them to the action of electric fields (rf and dc) projected on to four collinear rod structures [92]. Ions follow an oscillating trajectory through the rod assembly, the spatial parameters of which depend on the m/z ratio. At a given ratio of rf to dc field, only ions of particular mass pass through the quadrupole.

The positive and negative ions exiting the mass analyzer are detected by a channeltron multiplier, which outputs a signal increased by up to 10^8 over the input. The mass analyzer and detector are controlled by an IBM PC through Intelligent Instrumentation data boards.

The SIMS system is operated under ultra-high vacuum conditions (10^{-10} mbar) which is obtained by a diffusion pump backed by a rotary pump.

In our SIMS facility, the primary ion beam is produced by a differentially pumped noble gas ion gun, which consists of an electron impact ion source and a gun column. Electrons are emitted from a hot thermionic filament in the ion source and accelerated toward an ionization region. An appropriate gas, for example Xe, is injected into the region and is ionized by collision with the electrons. Using an electric field, the resulting positive ions are extracted out of the ionization region toward the gun column, where they are focused and accelerated toward the target.

The sample to be analyzed is mounted on a sample holder which can be locked on to a sample magazine. The sample magazine can hold up to six samples, and the position of a sample in the analysis chamber is adjustable by the manipulator.

4.3 Sample preparation and characterization

Square panels of 7075-T6 aluminum (1 cm^2) were degreased and acid etched before coating with γ-GPS solution (1 vol% formed by dissolving monomer in an equivolume mixture of distilled water and methanol). Three main samples are referred to below. Sample A is a blank sample prior to coating with γ-GPS (i.e. the alloy after etching); sample B is formed from sample A by applying the γ-GPS solution drop-by-drop until a thick layer of polymer is formed; sample C gives the γ-GPS/substrate interface formed by dipping sample A in the γ-GPS solution for 5 min followed by air drying. XPS spectra were measured with a Leybold MAX200 spectrometer using the unmonochromatized AlKα source (1486.6 eV) operated at 15 kV, 20 mA with pressure in the analysis chamber around $6x10^{-9}$ mbar. The

biased spectra were obtained by applying an external potential of -93 V through the sample holder, and then, after measurement, mathematically shifting the energy scale back by 93 eV [85]. Static SIMS was performed with a xenon primary beam (5 keV impact energy), for which a current of 0.2 nA irradiated a square area (6.25 mm^2) on the samples. Adhesion tests were conducted as described in Section 3.1.2.

4.4 Results and Discussion

4.4.1 XPS study

All three samples (A, B and C) were analyzed by XPS to give an indication of elemental composition and film thickness prior to a static SIMS analysis. A very thin film is required in order to see the interface by static SIMS since this technique has essentially a one monolayer sampling depth. An XPS survey spectrum from the blank alloy is shown in Figure 4.3(a), where Al, O, C and Zn are detected. The carbon is mainly from airborne contamination. It is not surprising that Zn was present since the 7075-T6 aluminum alloy contains about 6% of this metal. However, no Si was found on the blank alloy. Thus it is safe to conclude that any Si detected from the primed samples comes from the silane.

For sample B, on the contrary, Si was seen in the survey spectrum, as well as O and C. But Al was not detected. This indicates that sample B is completely covered by a layer of γ-GPS. The thickness of this layer is larger than the XPS sampling depth so the aluminum alloy substrate cannot be detected.

The XPS survey scan from sample C (Figure 4.4(a)) detects Si and Al, which shows that the metal interface can be probed by XPS. Further investigation used the bias potential

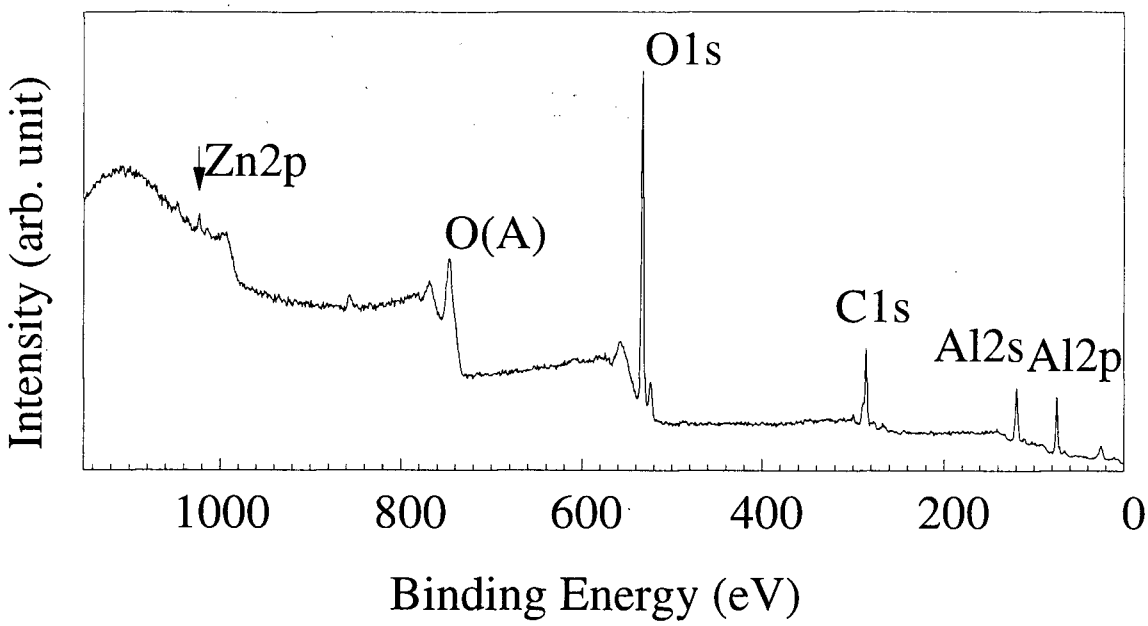

(a) sample A

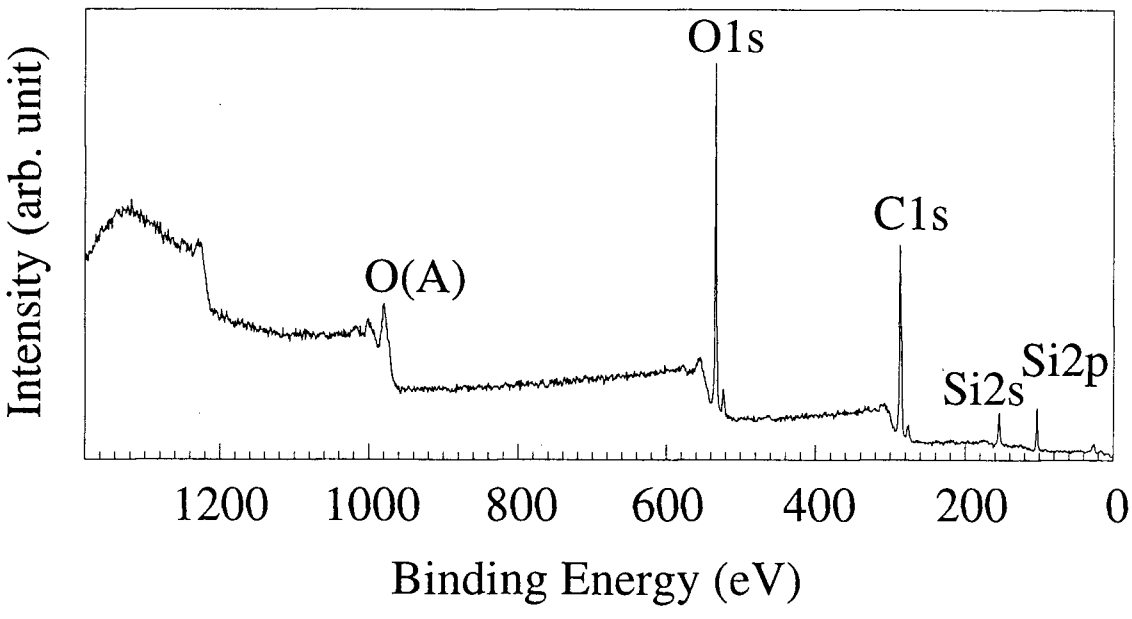

(b) sample B

Figure 4.3 XPS survey spectra for samples A and B

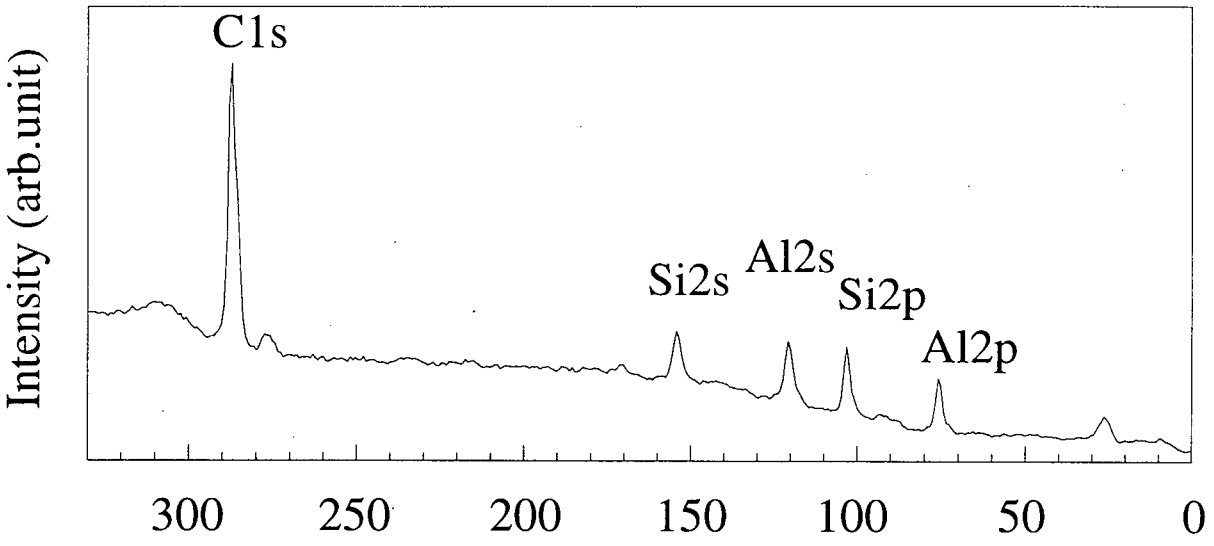

(a) Survey scan

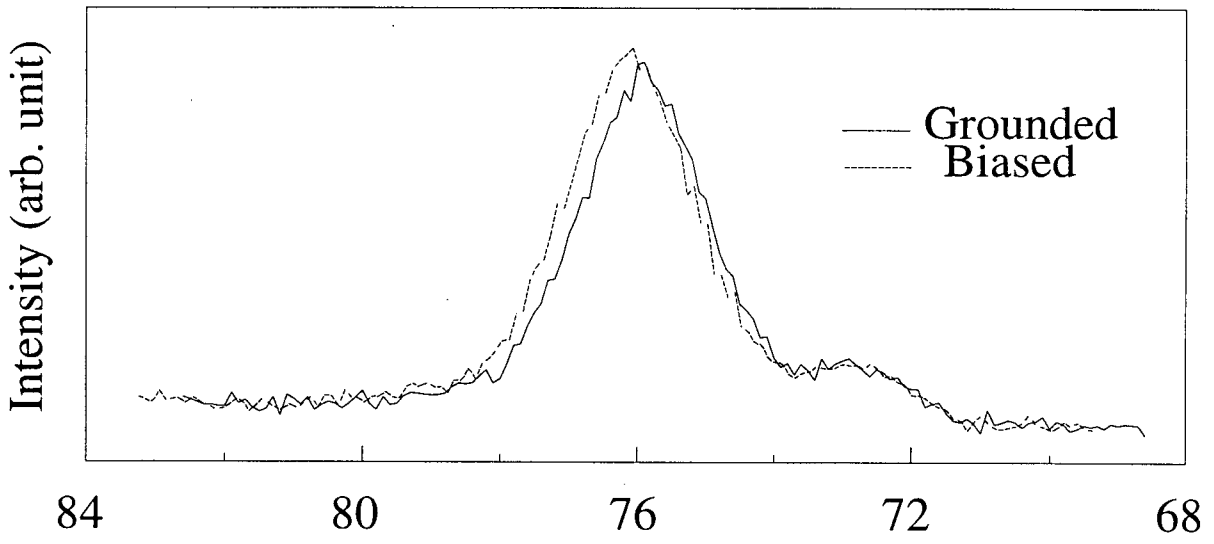

(b) Narrow scan of AL2p for GPS/Al interface

Figure 4.4 XPS survey and narrow scans for sample C

Table 4.2 Sample descriptions for silane studies

Code	Chemical type	Method of preparation
A	blank alloy	7075-T6 aluminum alloy panel degreased in acetone, rinsed in distilled water and etched
B	polymerized γ-GPS layer	sample A covered by thick γ-GPS layer (applied drop by drop)
C	γ-GPS/Al interface	sample A dipped in γ-GPS solution for 5 min and air dried

technique, for which narrow scan Al2p spectra are shown in Figure 4.4(b). The peaks at about 76 eV are assigned to oxide, whereas those at about 73 eV are assigned to the metallic form of Al. If a silane treated sample is in good electrical contact with the metal substrate, the Al2p peak for the grounded and biased spectra should overlap after correcting for the bias voltage. However for sample C, when the metal peaks overlap, an appreciable shift of the oxide peak can be observed. This implies that some oxide has different electrical properties from the rest of the aluminum oxide. A possible explanation is that some Al-O-Si chemical bonding formed between aluminum alloy and γ-GPS changes the electrical properties of the topmost aluminum oxide.

4.4.2 Static SIMS studies

Relevant positive ion static SIMS spectra are reported in Figure 4.5. The spectrum from sample A in Figure 4.5(a) is made up of Al^+ (mass 27) and CH fragments, the latter being indicative of the commonly observed hydrocarbon contamination. Since $C_2H_3^+$ and $C_2H_5^+$ fragments are usually comparable in intensity, only part of the mass 27 peak can be assigned to $C_2H_3^+$. The small peak as mass 28 may be AlH^+ (Si is considered less likely since no Si was detected by XPS). Sample B experienced charging under ion bombardment, and the spectrum in Figure 4.5(b) was obtained with operation of an electron flood gun (500 eV) to compensate. The signals obtained are fairly weak; nonetheless peaks from Si^+ and $SiOH^+$, and possibly $SiCH_3^+$, are evident in the spectrum. The presence of $SiOH^+$ is consistent with expectation from the γ-GPS polymerization [83]. There should be no contribution at mass 27 from Al^+ given the thickness of the γ-GPS layer, but hydrocarbon fragments, in part from the γ-GPS backbone, are clearly present.

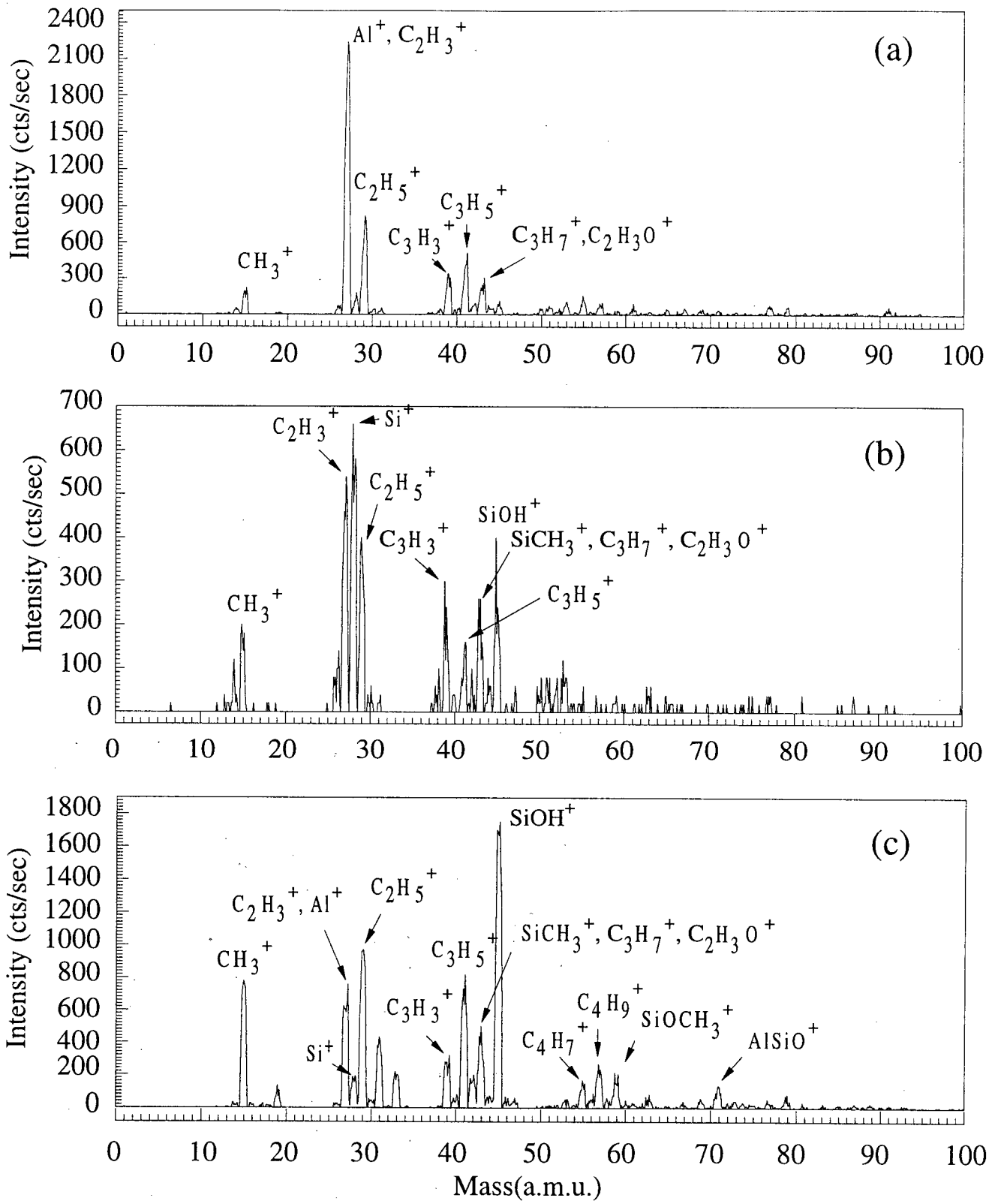

Figure 4.5 Positive SIMS spectra from: (a) sample A, (b) sample B and (c) sample C

Figure 4.5(c) shows the static SIMS spectrum for sample C. No sample charging was evident, thereby supporting the belief that the γ-GPS layer is very thin. The most prominent peak is at mass 45 ($SiOH^+$ from the γ-GPS polymerization), but there are additionally Si^+, $SiCH_3^+$, $SiOCH_3^+$ and hydrocarbon fragments from the backbone. Masses 27 and 29 have comparable heights, so it is not clear how much of the peak at mass 27 originates from Al^+. The spectrum also contains a small but definite peak at mass 71. This is not considered likely to originate with C_5 fragments for which masses 65, 67 and 69 could be expected [80, 93]. No significant peak is seen at 71 for either sample A or B, and therefore its presence in sample C appears intrinsic to the γ-GPS/Al interface. The most probable assignment is as $AlSiO^+$, in analogy with the observation of the $FeSiO^+$ species made by Gettings and Kinloch [83] from a γ-GPS/steel interface. The presence of $AlSiO^+$ in the SIMS spectrum is consistent with some direct Al-O-Si bonding at the interface. Interestingly, static SIMS characterizations of other thin-layer γ-GPS/Al samples, which because of differences in preparation did not show the extra structure in the Al2p spectrum from the bias potential test, have so far failed to detect significant structure at mass 71.

4.4.3 Adhesion test

An empirical probe of the effectiveness of the bonding at the γ-GPS/Al interface was made with a conventional adhesion test. Figure 4.6 shows schematic diagrams illustrating the cross sections of samples A and B before and after the adhesion test.

Although the only difference between samples A and C is the γ-GPS treatment, their behavior in the adhesion test are quite different. Sample A fractures between the paint and Al alloy substrate. However, the breakage in sample C occurred within the glue itself. It is clear

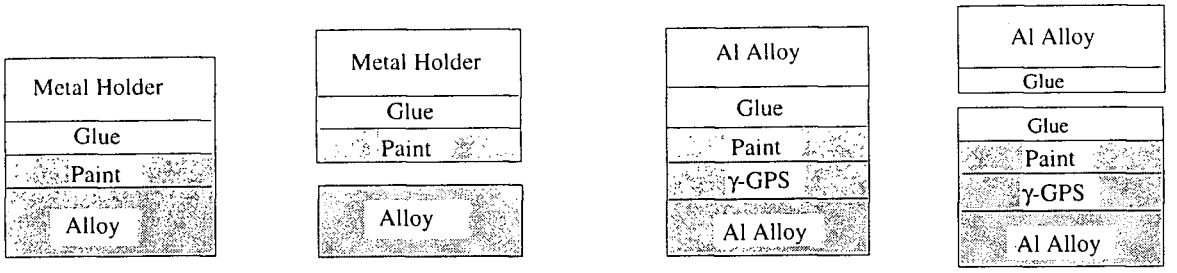

(a) Sample A before adhesion test

(b) Sample A after fracture

(c) Sample C before adhesion test

(d) Sample C after fracture

Figure 4.6 Adhesion tests for samples A and C

that without γ-GPS, there is very poor adhesion between the blank Al alloy and the paint. The γ-GPS substantially improves the adhesion so suggesting that γ-GPS bonds tightly to both the aluminum alloy and the paint. This is probably due to covalent bonding at the aluminum alloy interface while the deposited γ-GPS network may mechanically trap the paint through increased Van der Waals interactions.

4.5 Concluding remarks and future work

The observation with static SIMS from a γ-GPS/Al interface of structure at mass 71, which appears interpretable as $AlSiO^+$, provides circumstantial support for the direct Al-O-Si interfacial bonding that was postulated previously from observations with the XPS bias potential technique [84]. Such surface science characterizations appear to have considerable value for developing better understandings of the adhesive bond in macroscopic systems. Additional work with vibrational spectroscopy (e.g. FTIR) should also provide additional information in this area, and complement that from XPS and SIMS.

The present study focused on a particular γ-GPS/Al interfacial system, primarily to test our ability to identify these bonding effects. Clearly there will be great interest in extending such work to a range of silanes (e.g. others shown in Table 4.1), as well as to different metals including their various pretreatments.

References

[1] R.G. King, "Surface Treatment and Finishing of Aluminum" (Pergamon Press, 1988)

[2] S. Wernick, R. Pinner and P.G. Sheasby, "The Surface Treatment and Finishing of Aluminum and Its Alloys" (Finishing Publication, Teddington, 1987)

[3] T. Biestek and J. Weber, "Conversion Coatings" (Portcullis Press, Redhill, 1976)

[4] L.L. Sheir, R.A. Jarman and G.T. Burstein, "Corrosion", Vol.2, Third Ed. (Butterworth-Heinemann Ltd. 1994)

[5] R.Stricklen, Mater. and Meth. **35** (1952) 91

[6] J. Lindsay, Plat. & Surf. Finish. **84** (1997) 24

[7] British Patent 8667 (1906)

[8] S. Yonezaki, M. Kamata and K. Terayama, Interfinish 68 Proceedings (1968)

[9] A. Neuhaus and M. Gebhardt, Werkstoff und Korrosion **17** (1966) 493

[10] S. Spring, "Preparation of Metals for Painting" (Reinhold Publishing Co., New York, 1965)

[11] W. Rausch, " The Phosphating of Metals" (Finishing Publication, Teddington, 1990)

[12] T. Biestek and J. Weber "Conversion Coatings" (Portcullis Press, Redhill,1976)

[13] J.F. Ying, M.Y. Zhou, B.J. Flinn, P.C. Wong, K.A.R. Mitchell and T. Foster, J. Mat. Sci. **31** (1996) 565

[14] A. Turuno, K. Toyose, H. Fujimoto, Kobelco Tech. Rev. **11** (1991) 14

[15] D.B. Freeman, " Phosphating and Metal Pre-treatment" (Industrial Press Inc., New York, 1986)

[16] T. Goto, Jpn. Kakai Tokko Koho JP 04,41,667 [92 41,677]

[17] M.D. Vlasov, A.N.kolotusha, M.G. Naumov et al, U.S.S.R. SU 1,726,559

[18] G. Krebs, G. Reinhard, U. Rammelt et al, Ger DD 299,320

[19] K. Yamada, Jpn. Kakai Tokko Kono JP05,115,842 [93,115,842]

[20] W.F. Heung, Y.P. Yang, P.C. Wong, K.A.R. Mitchell and T. Foster, J. Mat. Sci. **29** (1994) 3653

[21] J.F. Ying, B.J. Flinn, M.Y. Zhou, P.C. Wong, K.A.R. Mitchell and T. Foster, Prog. Surf. Sci. **50** (1995) 259

[22] J.L. Fang, J. Fang, and X.R. Ye, Materials Protection **24** (1991) 8

[23] O. Furuyama, H. Ishii, Interfinish 92, Int. Congr. Surf. Finish. **2** (1992) 661

[24] K. Ogawa, I. Kotani, Aichi Kogyo Gijutsu Senta HoKoku **29** (1993) 45

[25] W.F. Heung, P.C. Wong, K.A.R. Mitchell, T. Foster, J. Mat. Sci.Lett **14** (1995) 1461

[26] D.B. Freeman, " Phosphating and Metal Pre-treatment" (Industrial Press Inc., New York,1986)

[27] U.B. Nair, M. Subbaiyan, Met. Finish. **91** (1993) 1

[28] M.R. Fardi in "Progress in the Understanding and Prevention of Corrosion" Vol.1 edited by J.M. Costa and A.D. Mercer (The Institute of Materials, 1993)

[29] U.B. Nair, M. Subbaiyan, J. Mat. Sci. **30** (1995) 2108

[30] G.N. Bhar, N.C. Debnath and S. Roy, Surface and Coating Technology **35** (1988) 171

[31] M.O.W. Richardson and D.B. Freeman, Trans. Inst. Met. Finish **64** (1986) 16

[32] A. Turuno, K. Toyose, H. Fujimoto, Kobelco Tech. Rev. **14** (1991) 11

[33] R.W. Zurilla and V. Hospandaruk, Trans. SAE 780187, **87** (1978) 762

[34] L. Fedrizzi and F. Marchetti, J. Mat. Sci., **26** (1991) 1931

[35] J.A. Treverton, A.Bosland and J. M. Brown, Corr. Sci. **30** (1990) 1159

[36] R.S. Alwitt and G.E.Thompson, J. Electrochem. Soc. **86** (1986) 217

[37] J.S. Crompton, P.R. Andrews and E. McAlpine, Surf Interface Anal. **13** (1988) 160

[38] H. Windawi and F.L. Ho, "Applied Electron Spectroscopy For Chemical Analysis" (John Wiley & Sons, New York, 1982)

[39] K. Kiss and M. Coll-Palagos, Corrosion **43** (1987) 8

[40] T. Sugama, L.E. Kukacka, N. Carciello and J.B. Warren, J. Appl. Polym. Sci. **30** (1985) 2137

[41] G. Rudolph, H. Hansen, Trans.Inst. Met. Finish. **50** (1972) 33

[42] J.F. Watts, An Introductory to Surface Analysis by Electroscopy (Oxford University Press, Oxford, 1990)

[43] H. Hertz, Annal Phys. **31** (1887) 982

[44] A. Einstein, Annal Phys. **17** (1905) 132

[45] H. Robinson and W.F. Rawlinson, Phil. Mag. **28** (1941) 277; H. Robinson, Phil. Mag. **50** (1925) 241

[46] K. Siegbahn, C.N. Nording, A. Fahlman, R. Nordberg, K. Hamrin, J. Hedman, G. Johansson, T. Bermark, S.E. Karlsson, I. Lindgren and B. Lindberg, "ESCA: Atomic, Molecular and Solid State Structure Studied by Means of Electron Spectroscopy" (Almqvist and Wiksells, Uppsala, 1967)

[47] K. Siegbahn, Prix Nobel, **114** (1981, Pub. 1982); Science, **217** (1982) 111; Rev. Mod. Phys., **54** (1982) 709

[48] C.R. Brundle and M.W. Roberts, Proc. Roy. Soc. **A331** (1972) 383

[49] N.H. Turner, in "Investigations of Surfaces and Interfaces", edited by B.W. Rossiter and R.C. Baetzold (John Wiley & Sons, New York, 1993)

[50] Y.M. Wang, Ph.D. thesis, University of British Columbia, 1996

[51] Perkin Elmer Co. " Handbook of X-ray photoelectron spectroscopies" (1979)

[52] K. Siegbahn, C. Nordling, A. Fahlman et al, Nova Acta Regiae Societatis Sci. Upsallensis, Seroes 4, **20** (1967) 1

[53] MAX200 User Manual (Leybold, Koln, Germany)

[54] D.A. Shirley, Phys. Rev. **B5** (1972) 4709

[55] C.S. Fadley, Prog. Surf. Sci. **16** (1984) 275

[56] B.J. Tielsch and J.E. Fulghum, Surf. Interface Anal. **24** (1996) 422

[57] H. Windawi, J. Electron Spectrosc. **22** (1981) 373

[58] Y.L. Leung, M.Y. Zhou, P.C. Wong, K.A.R. Mitchell and T. Foster, Appl. Surf. Sci. **59** (1992) 23

[59] A.J. Pertsin and Y.M. Pashunin, Appl. Surf. Sci., **44** (1990) 171

[60] P.J. Goodhew and F.J. Humphreys, "Electron Microscopy and Analysis" (Taylor & Francis, London, 1988)

[61] J.F. Ying, M.Y. Zhou, B.J. Flinn, P.C. Wong, K.A.R. Mitchell and T. Foster, J. Mat. Sci. **31** (1996) 565

[62] D.B. Freeman, " Phosphating and Metal Pre-treatment" (Industrial Press Inc., New York, 1986)

[63] W.F. Heung, Y.P. Yang, P.C. Wong, K.A.R. Mitchell and T. Foster, J. Mat. Sci. **29** (1994) 1368

[64] J.F. Ying, B.J. Flinn, M.Y. Zhou, P.C. Wong, K.A.R. Mitchell and T. Foster, Prog. Surf. Sci. **50** (1995) 259

[65] J.B. Lakeman, D.R. Gabe and M.O.W. Richardson, Trans. Inst. Met. Fin. **55** (1977) 47

[66] D.R. Lenard, Esquimalt Defence Research Detachment, unpublished observations.

[67] M.Y. Zhou, Department of Chemistry, UBC, unpublished observations.

[68] D. Briggs and M.P. Seah, "Practical Surface Analysis" (John Wiley & Sons, Chichester 1990)

[69] T.S. Narayanan, J. Electrochem. Soc. India **41** (1992) 1

[70] Y. Long, Materials Protection **26** (1993) 4

[71] E.P. Plueddemann, "Silane Coupling Agents", (Plemum, New York, 1991)

[72] B. Muller and I. Foster, Corrosion Science **38** (1996) 7

[73] A.D. Wilson, J.W. Nicholson and H.J. Prosser, "Surface Coatings" (Elsevier Science Pub., London, 1987)

[74] H. Ishida and J.L. Koenig, J. Colloid Interf. Sci. **64** (1978) 565

[75] F.J. Boerio and J.W. Williams, "Applications of Surface Science,Vol.7" (North Holland Publishing Co., Amsterdam, 1981)

[76] M.R. Rosen, J. Coating Tech. **50** (1978) 70

[77] H.H. Sung and C.S.P. Sung, Org. Coat. Plast. Chem. **42** (1980) 743

[78] S.G. Hong and F.J. Boerio, Surf. Interface Anal. **21** (1994) 650

[79] J. Comyn, D.P. Oxley, R.G. Pritchard and C.R. Werret, J. Adhesion **28** (1989) 171

[80] W.J. Van Ooij and A. Sabata, Surf. Interface Anal. **19** (1992) 101; **20** (1993) 475

[81] M.R. Horner, F.J. Boerio and H.M. Clearfield, J. Adhes. Sci. Technol. **6** (1992) 1

[82] R.G. Schmidt, J.P. Bell and A. Garton, J. Adhes. **27** (1989) 127

[83] M. Gettings and A.J. Kinloch, J. Mat. Sci. **12** (1977) 2511

[84] Y.L. Leung, M.Y. Zhou, P.C. Wong, K.A.R. Mitchell and T. Foster, Appl. Surf. Sci. **59** (1992) 23

[85] Y.L. Leung, Y.P. Yang, P.C. Wong, K.A.R. Mitchell and T. Foster, J. Mat. Sci. Lett. **12** (1993) 844

[86] K.J. Hook, T.J. Hook, J.H. Wandass and J.A. Gardella, Appl. Surf. Sci. **44** (1990) 29

[87] A. Benninghoven, F.G. Rudenauer and H.W. Werner, "Secondary Ion Mass Spectrometry" (John Wiley & Sons Inc, New York,1987)

[88] S.E. Asher in "Microanalysis of Solid", edited by B.G. Yacobi, D.B. Holt and L.L. Kazmerski (Plenum Press, New york, 1994)

[89] B.M. Rossiter and R.C. Baetzold, "Investigations of Surfaces and Interfaces -Part B" (John Wiley & Sons Inc., New York, 1993)

[90] A. Benninghoven, Z. Phys. **230** (1970) 403

[91] P.D. Prewett and D.K. Jeffries, Inst. Phys. Conf. Ser. **54** (1980) 316

[92] K.L. Busch in "Ion Spectroscopies For Surface Analysis", edited by A.W. Czanderna and D.M. Hercules (Plenum Press, New York, 1991)

[93] A. Brown and J.C. Vickerman, Surf. Interface Anal. **8** (1986) 75

[94] Instruction Manual for Model S4100 Field Emission Scanning Electron Microscope, Hitachi Ltd., 1991